

Nodal liquid and *s*-wave superconductivity in transition metal dichalcogenides

B. Uchoa¹, G. G. Cabrera¹, and A. H. Castro Neto²

¹ Instituto de Física “Gleb Wataghin” Universidade Estadual de Campinas (UNICAMP), C. P. 6165, Campinas, SP 13083-970, Brazil

² Department of Physics, Boston University, 590 Commonwealth Ave., Boston, MA 02215

(Dated: July 17, 2004)

We explore the physical properties of a unified microscopic theory for the coexistence of superconductivity and charge density waves in two-dimensional transition metal dichalcogenides. In the case of particle-hole symmetry the elementary particles are Dirac fermions at the nodes of the charge density wave gap. When particle-hole symmetry is broken electron (hole) pockets are formed around the Fermi surface. The superconducting ground state emerges from the pairing of nodal quasi-particles mediated by acoustic phonons via a piezoelectric coupling. We calculate several properties in the *s*-wave superconducting phase, including specific heat, ultra-sound absorption, nuclear magnetic relaxation, thermal, and optical conductivities. In the case with particle-hole symmetry, the specific heat jump at the transition deviates strongly from ordinary superconductors. The nuclear magnetic response shows an anomalous in-plane anisotropy due to the broken rotational symmetry of the triple charge density wave state. The loss of lattice inversion symmetry in the charge density wave phase leads to anomalous coherence factors in the optical conductivity and to the appearance of an absorption edge at the optical gap energy. Furthermore, optical and thermal conductivities display anomalous peaks in the infrared when particle-hole symmetry is broken.

PACS numbers: 74.20.Mn, 71.10.Hf, 71.45.Lr

I. INTRODUCTION

The quasi two-dimensional (2D) transition metal dichalcogenides (TMD) 2H-TaSe₂, 2H-TaS₂ and 2H-NbSe₂ are layered compounds where *s*-wave superconductivity coexists with a charge density wave (CDW)^{1,2} at low temperatures, and whose transport properties are highly anisotropic in the high temperature CDW phase³. There is a vast literature reporting anomalous effects in the CDW phase, including, non-linear Hall effect, anomalous impurity effects in the superconducting (SC) phase⁴, stripe phases⁵, and different regimes of commensurability⁶. Recent angle resolved photoemission experiments (ARPES) reveal that the quasi-particles of TaSe₂ have a marginal Fermi liquid (MFL) lifetime⁷. This scenario becomes more exciting by the verification that some of the physical properties of TMD, such as the linear growth of the normal resistivity with temperature³, and the strong anisotropy in the in-plane and out-of-plane transport are similar to the same properties in the high temperature superconductors (HTc). HTc do not show a CDW gap but a *d*-wave *pseudo-gap* coexisting with the superconducting phase. In both cases, the transport and thermodynamic properties are weakly dependent on the application of external fields in the normal/pseudo-gap phase, and strongly dependent on them in the superconducting phase⁸. Furthermore, the application of pressure in TMD favors the superconductivity and suppresses the CDW phase⁹, in a close analogy with the HTc phase diagram of temperature versus doping. Differently from the HTc, however, the TMD are very clean materials. The anomalous TMD properties are sample independent and can help to clarify the physics behind a whole class of low-dimensional superconductors.

The interpretation of the experimental data in TMD is however still very controversial. Within the Peierls theory, the CDW gap formation in 1D systems is usually due to nested Fermi surfaces. In 2D systems, the nesting is not perfect and some parts of the Fermi surface may not be gaped. Early band structure calculations¹⁰ indicated that the Γ centered sheets (S_I) are nested with the K centered ones (S_{II}) by the \mathbf{Q}_i ($i = 1, 2, 3$) wavevectors of the triple-CDW (see Fig. 1). The value of the CDW wave-vector, $|\mathbf{Q}_i| \sim \frac{1}{3}\Gamma K$, measured by neutron diffraction^{11,12}, and recent scanning tunneling microscopy (STM) experiments^{13,14,15} confirm the plausibility of a nesting scenario. An alternative theory proposed by Rice and Scott¹⁶ is based on a Fermi surface independent CDW mechanism, where the CDW wavevectors connect the saddle points (indicated in Fig. 1 around $\frac{1}{2}\Gamma K$) of the transition metal *d*-bands, generating a logarithmic divergence in the electronic susceptibility. However, the saddle point energy in NbSe₂ is too large (~ 50 meV) in comparison to the CDW ordering thermal energy $k_B T_{CDW} \sim 3$ meV to allow a saddle point driven instability¹⁷. In TaSe₂, however, ARPES has observed an extended saddle band along ΓK . This band is nearly flat and closer to the Fermi energy than the band calculations predicted^{18,19}. As the saddle points are not well defined in this case, it is questionable to justify the CDW wave-vector measured with neutrons by some mechanism related to special parts of the saddle bands. More experimental studies are required to elucidate this point.

If on one hand these arguments seem to rule out at least a conventional saddle point mechanism, consensus on the origin of the CDW instability has not been reached. STM scans at 4.2 K in TaSe₂, TaS₂ and NbSe₂ show that the amplitude of the CDW gap is $\Delta_{CDW} \sim 80, 50$, and 34 meV, respectively²⁰. The

ability of ARPES to measure the superconducting gap $\Delta_s \sim 1$ meV $\ll \Delta_{CDW}$ in NbSe_2 , combined with the complete failure of ARPES to detect traces of the CDW gap in the Brillouin zone of TaSe_2 and NbSe_2 ^{7,21} were interpreted as an evidence that the Fermi surface is weakly covered by the CDW. We observe that the ARPES results seem to be in contradiction with the STM data, and cannot explain the non-Fermi liquid transport in the TaSe_2 crystal. One possibility is that the ARPES data are obscured by the strong dependence of CDW gap with the directions of the Brillouin zone combined with the formation of pockets in the points of the Fermi surface where $\Delta_c(\mathbf{k}) = 0$ ($\max[\Delta_c(\mathbf{k})] = \Delta_{CDW}$). Another possibility is that the ARPES electronic dipole matrix elements vanish for certain states in the CDW phase due to the broken spacial inversion symmetry (detected in neutron scattering¹²) forbidding the observation of some bands.

The strong resemblance of the normal CDW phase resistivity of TaSe_2 with the HTc²² and the anomalous quasi-particle life-time, given by the inverse of the imaginary part of the electronic self-energy⁷ $\text{Im} \Sigma(k_F, \omega) \propto \tau_0^{-1} + b|\omega|$, indicates that a marginal Fermi liquid theory²³ should be developed as the basis of a minimal model unifying the CDW and superconducting phases in TaSe_2 . The experimental verification that $k_B T_{CDW} \ll \Delta_{CDW}$ for all the TMD (in TaSe_2 for example, $k_B T_{CDW} \sim 120$ K ~ 12 meV) gives a good indication that a strong coupling CDW theory is required.

One of us (A.H.C.N.)²⁴ has recently proposed a unified picture for the CDW and SC phases where the elementary particles are Dirac fermions that are created in the region where the CDW gap vanishes, leading to the generation of a nodal liquid. According to neutron diffraction studies, the inversion center of the crystal is lost in the CDW phase¹², allowing for the possibility of piezoelectric effects. In a system with nodal quasiparticles, the piezoelectric coupling is a marginal coupling from the renormalization group (RG) point of view, while the usual electron-phonon coupling is irrelevant under the RG²⁵. Based on a *tight-binding* description of the electronic orbitals²⁶, and on the assumption of imperfect nesting between different Fermi surface sheets, the model of ref. [24] proposes a *f*-wave symmetry CDW gap, with lobes along the saddle point directions, and six nodes at the points where the gap is zero (see Fig. 1). The proposed CDW gap is odd in the Brillouin zone, due to the symmetry of the electron-phonon coupling²⁴, and due to the absence of inversion symmetry in the CDW phase, changing sign in each node. The superconductivity emerges from Cooper pairing between the Dirac fermions mediated by acoustic phonons via a piezoelectric coupling. We propose that the Fermi surface is fully gaped by the superposition of the CDW and the *s*-wave superconducting (SC) order parameters. This model is able to correctly explain some of the anomalous properties of the TMD like the marginal quasi-particles life-time in TaSe_2 , the dependence of the normal-superconducting phase transition with the lattice parameters, and the

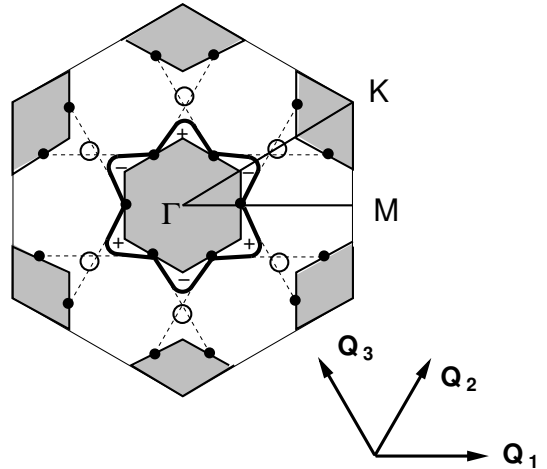


Figure 1: Schematic representation of the TMD Fermi surface. The Γ centered sheet (S_1) is nested with the K centered ones (S_{II}) by the CDW wavevectors \mathbf{Q}_i . A CDW gap develops in the two sheets, except in the nodal points, indicated by the black filled circles. The empty circles are the saddle points. The thick solid line around the S_1 sheet is the proposed CDW gap. The dashed lines indicate the nodes connected by \mathbf{Q}_i .

metallic behavior of the resistivity in the CDW phase²⁴.

The geometry of the proposed CDW gap is similar to the Brillouin zone of graphite, where the nodes represent the points where the conduction and valence π -bands cross each other²⁷. In contrast to graphite, the lattice inversion symmetry is broken in the distorted phase, and the piezoelectricity can arise. As it is usually observed in insulators, since metals screen the polarization fields, one may ask: is actually possible to find piezoelectricity in a superconductor? To answer this question, we should consider first that in a nodal liquid the density of states (DOS) goes to zero in the nodes, and therefore the electrons cannot effectively screen electric fields. Hence, one can conciliate a metallic theory (with gapless quasi-particle excitations) with piezoelectricity. The rigorous vanishing of the DOS at the Fermi surface, however, is not essential for the piezoelectricity to appear. It is sufficient to consider that the electrons of low lying momentum (for example, in a small pocket around the nodes) are "slow" enough to couple with the acoustic phonons of the polarized lattice.

If the piezoelectricity and the metallic character are not mutually excluding, it remains the question of how the polarization vector affects the phase coherence of the condensate. The answer to this question can be found in the collective modes. The electromagnetic gauge invariance of the superconducting state is provided by the longitudinal response of the collective excitations, that screen the electrons through a cloud of virtual plasmons²⁸. Only the plasmons respond to the longitudinal fields and give rise to screening. Since the piezoelectricity involves electric fields only, it does not affect the phase coherence of the electrons. In a previous

work²⁹, we have shown by means of a semi-classical calculation that piezoelectricity is not only consistent with the stability of the condensate as it is possibly behind the quantum critical points (QCP) observed experimentally in the TaSe₂ phase diagram, separating the $T = 0$ commensurate phases from the stripe phase as a function of the applied pressure.

The organization of the paper is as follows: in sec. II we introduce the model Hamiltonian of the CDW and superconducting phase; in sec. III we derive the superconducting gap equation; sec. IV is devoted to the thermodynamics of the superconducting phase while in sec. V we calculate the acoustic attenuation rate and the NMR response; in sec. VI we calculate the optical and thermal conductivities; in sec. VII we discuss the Meissner effect; sec. VIII contains our conclusions.

II. THE HAMILTONIAN

The nodal system is composed of two subsystems defined by the nodes of the CDW state which are connected by the triple-CDW wavevectors \mathbf{Q}_i ($i = 1, 2, 3$). It is convenient to introduce the spinors

$$\Psi_{i,\sigma}(\mathbf{k}) = \begin{pmatrix} c_{\mathbf{k},\sigma} \\ c_{\mathbf{k}+\mathbf{Q}_i,\sigma} \end{pmatrix} = \begin{pmatrix} \psi_{+,i,\sigma}(\mathbf{k}) \\ \psi_{-,i,\sigma}(\mathbf{k}) \end{pmatrix},$$

where $+, -$ indicate the two nodal spaces, where $c_{\mathbf{k},\sigma}^\dagger$ ($c_{\mathbf{k},\sigma}$) are creation (annihilation) operators for electrons with momentum \mathbf{k} and spin $\sigma = \uparrow, \downarrow$. The electronic Hamiltonian in the normal CDW phase is composed of two terms,

$$H_{CDW} = H_e + H_{e-c}.$$

H_e is the Hamiltonian of the free electrons in the vicinity of the nodes,

$$\begin{aligned} H_e &= \sum_{\mathbf{k},\sigma,i} \left[\epsilon_{\mathbf{k}} c_{\sigma,\mathbf{k}}^\dagger c_{\sigma,\mathbf{k}} + \epsilon_{\mathbf{k}+\mathbf{Q}_i} c_{\sigma,\mathbf{k}+\mathbf{Q}_i}^\dagger c_{\sigma,\mathbf{k}+\mathbf{Q}_i} \right] \\ &= \frac{1}{2} \sum_{\mathbf{k},a,b,\sigma,i} \psi_{a,i,\sigma}^\dagger(\mathbf{k}) \left[(\epsilon_{\mathbf{k}} + \epsilon_{\mathbf{k}+\mathbf{Q}_i}) \eta_0^{ab} \right. \\ &\quad \left. + (\epsilon_{\mathbf{k}} - \epsilon_{\mathbf{k}+\mathbf{Q}_i}) \eta_3^{ab} \right] \psi_{b,i,\sigma}(\mathbf{k}), \quad (1) \end{aligned}$$

where η_ν ($\nu = 0, 1, 2, 3$) are Pauli matrices that act in the nodal indexes $a, b = \pm$, and $\epsilon_{\mathbf{k}}$ is the free electron dispersion. In our convention, η_0 is the identity and $\nu = 1, 2, 3$ indexes the x, y, z directions, respectively. The second term in the Hamiltonian, H_{e-c} , is the CDW exchange Hamiltonian between electrons situated in two different nodes connected by \mathbf{Q}_i ,

$$\begin{aligned} H_{e-c} &= \sum_{i,\mathbf{k}} \Delta_{c\mathbf{k}} c_{\mathbf{k}\sigma}^\dagger c_{\mathbf{k}+\mathbf{Q}_i} + h.c. \\ &= \sum_{i,\mathbf{k},\sigma,a,b} \Delta_{c\mathbf{k}} \psi_{a,i,\sigma}^\dagger(\mathbf{k}) \eta_1^{ab} \psi_{b,i,\sigma}(\mathbf{k}). \quad (2) \end{aligned}$$

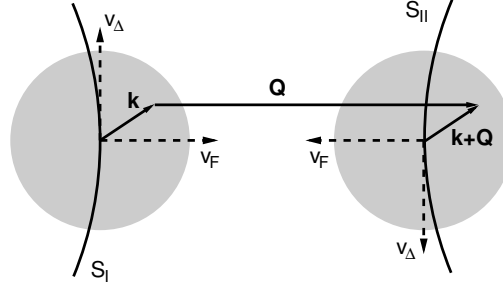


Figure 2: Nesting condition in the two sheets S_I and S_{II} of the TMD Fermi surface. The momentum \mathbf{k} outside S_I is mapped by a CDW wavevector displacement into $\mathbf{k} + \mathbf{Q}$, inside S_{II} . As the free electron dispersion $\epsilon_{\mathbf{k}}$ is odd with respect to the Fermi surface sheets, we have $\epsilon_{\mathbf{k}} = -\epsilon_{\mathbf{k}+\mathbf{Q}}$.

where $\Delta_{c\mathbf{k}}$ is the CDW gap, with odd-parity in the nodal space due to the loss of the lattice inversion symmetry. This term arises from the scattering of the electronic wave function by the CDW periodic superstructure.

Applying the *nesting* condition $\epsilon_{\mathbf{k}} + \epsilon_{\mathbf{k}+\mathbf{Q}} = 0$, (see Fig. 2) in Eq. (1), and taking the long-wavelength, low-energy limit, the Hamiltonian in the CDW phase reads,

$$H_{CDW} = \sum_{\mathbf{k},\sigma,i} \Psi_{i,\sigma}^\dagger(\mathbf{k}) [v_F k_{\perp} \eta_3 + v_{\Delta} k_{\parallel} \eta_1] \Psi_{i,\sigma}(\mathbf{k}), \quad (3)$$

where k_{\perp} and k_{\parallel} are the momentum components in the normal and parallel directions to the Fermi surface, respectively, v_F is the Fermi surface velocity and, $v_{\Delta} = \frac{\partial \Delta_c}{\partial k_{\parallel}}$. The CDW elementary excitations around the nodes are therefore fermions which follow the two-dimensional massless Dirac Hamiltonian, similarly to the two-band electronic description of graphite²⁷.

The broken lattice inversion symmetry due to the CDW gap allows the piezoelectricity in the crystal. We propose that the electron-phonon coupling is piezoelectric, giving rise to a pairing of Dirac fermions in the singlet state through the triple-CDW superstructure. In contrast with usual Cooper pairs, whose electrons are paired across the Fermi surface, these pairs are formed by electrons located in different nodes linked by a CDW wavevector \mathbf{Q}_i (see Fig. 1). The pairing approximation consists in assuming a condensate of pairs whose center of mass have momentum \mathbf{Q}_i and zero spin. This assumption clearly *violates* the time-reversal symmetry of the superconductor order parameter Δ_s . According to Anderson³⁰, the strong insensitivity of the BCS superconductors to impurities is due to the tendency of electrons to be in the state of highest possible degeneracy in the condensate, implying pairing each electron with its symmetric in spin and momentum. In such case, the scattering channels promote transitions between two degenerated states, keeping the system coherent. The absence of time reversal symmetry should destroy the condensate in the presence of a very small impurity concentration³¹.

In the case TMD, however, the CDW scattering does not affect the degeneracy of the condensate as far as the Dirac fermions Ψ_i living in different nodal subspaces (indexed by the three CDW directions $i = 1, 2, 3$) remain decoupled. For this reason, we may drop the i index from now on.

After tracing the phonons, the piezoelectric pair interaction has the form²⁴,

$$H_P = -g \sum_{\mathbf{k}, \mathbf{k}'} \sum_{a, b, c, d} \eta_2^{a b} \eta_2^{c d} \psi_{a, \uparrow}^\dagger(\mathbf{k}) \psi_{b, \downarrow}^\dagger(-\mathbf{k}) \times \psi_{c, \uparrow}(\mathbf{k}') \psi_{d, \downarrow}(-\mathbf{k}'),$$

where g is the coupling constant. The choice of the anti-symmetric Pauli matrix η_2 incorporates the broken symmetry of the superconducting gap. In the mean field approximation, the pairing Hamiltonian reads,

$$H_P = \sum_{\mathbf{k}} \sum_{a, b} \left[\Delta_s \psi_{a, \uparrow}^\dagger(\mathbf{k}) \eta_2^{a b} \psi_{b, \downarrow}^\dagger(-\mathbf{k}) + h.c. \right] + \frac{\Delta_s^2}{g} \quad (4)$$

where

$$\Delta_s = -g \sum_{\mathbf{k}} \sum_{a, b} \langle \psi_{a, \uparrow}(\mathbf{k}) \eta_2^{a b} \psi_{b, \downarrow}(-\mathbf{k}) \rangle \quad (5)$$

is the complex superconductor order parameter.

So far, we have discussed the problem with particle-hole symmetry, that is, the chemical potential μ is exactly at the Dirac point ($\mu = 0$). In order to include the situation where particle-hole symmetry is broken we have add to Eq. (3) a chemical potential term

$$H_\mu = -\mu \sum_{\sigma, a} \psi_{a, \sigma}^\dagger(\mathbf{k}) \psi_{a, \sigma}(\mathbf{k}). \quad (6)$$

This term introduces an electron ($\mu > 0$) or hole ($\mu < 0$) pocket around the Dirac point producing a finite density of states.

In order to diagonalize the problem it is convenient to extend the spinorial notation to the Nambu space

$$\Psi(\mathbf{k}) = \begin{pmatrix} \psi_{+, \uparrow}(\mathbf{k}) \\ \psi_{+, \downarrow}^\dagger(-\mathbf{k}) \\ \psi_{-, \uparrow}(\mathbf{k}) \\ \psi_{-, \downarrow}^\dagger(-\mathbf{k}) \end{pmatrix}, \quad (7)$$

with \mathbf{k} defined with respect to the nodes. We introduce a new set of Pauli matrices τ_μ which operates in the space $(\uparrow k, \downarrow -k)$. Denoting $\tau_\mu \eta_\nu$ as the tensor product between the Nambu and nodal spaces, it is not difficult to see that the full Hamiltonian is written as

$$H = \sum_{\mathbf{k}} \Psi^\dagger(\mathbf{k}) [v_F k_\perp \tau_0 \eta_3 + v_\Delta k_\parallel \tau_0 \eta_1 + \Delta_s \tau_1 \eta_2 - \mu \tau_3 \eta_0] \Psi(\mathbf{k}). \quad (8)$$

Notice that the gauge symmetry of the problem $\psi \rightarrow \psi e^{i\theta}$, and $\Delta_s e^{2i\theta} \rightarrow \Delta_s$, is broken at the mean-field level. With this notation, the SC order parameter is given by :

$$\Delta_s = -g \sum_{\mathbf{k}} \langle \Psi^\dagger(\mathbf{k}) \tau_1 \eta_2 \Psi(\mathbf{k}) \rangle. \quad (9)$$

The diagonalization of the Hamiltonian leads to four branches of excitations:

$$\pm E_{\mathbf{k}, \pm \mu} \equiv \pm \sqrt{(v_F \bar{k} \pm \mu)^2 + \Delta_s^2}, \quad (10)$$

where $\bar{\mathbf{k}} = \vec{k}_\perp + (v_\Delta/v_F) \vec{k}_\parallel$ is the in-plane anisotropic momentum, with $\bar{k} \equiv |\bar{\mathbf{k}}|$. In the normal phase, we identify two branches of excitations (we assume $\mu > 0$):

$$\pm E_{\mathbf{k}, \pm \mu} \xrightarrow{\Delta_s \rightarrow 0} \begin{cases} \pm v_F \bar{k} + \mu & \text{(hole-like branch)} \\ \pm v_F \bar{k} - \mu & \text{(particle-like branch)} \end{cases},$$

which are related to hole and particle-like pockets around the CDW nodes (for $\mu < 0$, the nomenclature is exchanged). The two branches are physically equivalent to each other, except for a constant equal to $-\sum_{\mathbf{k}} 2\mu$, integrated in the volume of the Dirac cone. The optical gap in the SC phase is $2\sqrt{\mu^2 + \Delta_s^2}$, as one can see from Fig. 3.

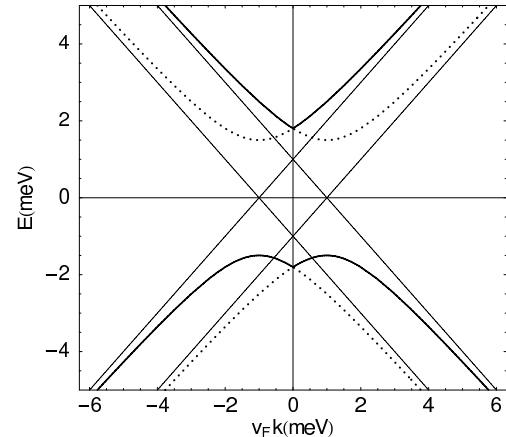


Figure 3: Dirac fermion dispersion in the pocket with the opening of the SC gap for $|\mu| = \frac{3}{2} \Delta_s = 1$ meV. Each band has two pocket branches indicated by the dotted and thick solid lines. The thin solid lines with the vertex above (below) the Fermi energy $E = 0$ represent the hole (particle)-like branches of the Dirac cone in the normal CDW phase.

III. THE GAP EQUATION

To calculate the gap self-consistently, we use the standard many-body Green's function method. Since Hamiltonian (8) has a quadratic form, $H = \sum_{\mathbf{k}} \Psi^\dagger \tilde{\omega} \Psi$, its

corresponding Green function in the 4×4 space is:

$$\overleftrightarrow{G}(\mathbf{k}, i\omega_n) = - \int_0^\beta d\tau e^{i\omega_n \tau} \langle T_\tau [\Psi \Psi^\dagger] \rangle = \left(i\omega_n - \overleftrightarrow{\omega}_\mathbf{k} \right)^{-1},$$

where T_τ is the time-ordering operator in imaginary time, ω_n are the fermionic Matsubara frequencies, $\beta = 1/(k_B T)$ is the inverse of temperature, k_B is the Boltzmann constant, and

$$\overleftrightarrow{\omega}_\mathbf{k} \equiv v_F \tau_0 \vec{\eta} \cdot \bar{\mathbf{k}} + \Delta_s \tau_1 \eta_2 - \mu \tau_3 \eta_0, \quad (11)$$

is the dispersion tensor with $v_F \vec{\eta} \cdot \bar{\mathbf{k}} \equiv v_F k_\perp \eta_3 + v_\Delta k_\parallel \eta_1$. Exploring the anti-commutative property of the Pauli matrices, the Green function which is systematically used in our calculation is:

$$\overleftrightarrow{G}(\omega_n, \mathbf{k}) = - \left(i\omega_n + \overleftrightarrow{\omega}_\mathbf{k} \right) \frac{\omega_n^2 + E'_\mathbf{k}^2 + 2\mu v_F \tau_3 \vec{\eta} \cdot \bar{\mathbf{k}}}{[\omega_n^2 + E_{\mathbf{k},\mu}^2][\omega_n^2 + E_{\mathbf{k},-\mu}^2]}, \quad (12)$$

where

$$E'_\mathbf{k}^2 \equiv v_F^2 \bar{k}^2 + \mu^2 + \Delta_s^2 = E_{\mathbf{k},\pm\mu}^2 - 2v_F(\pm\mu)\bar{k}.$$

Noting that $\langle \Psi_\alpha^\dagger(\mathbf{k}) \Psi_\beta(\mathbf{k}) \rangle$ is the retarded part of the Green function, $G_{\beta\alpha}(\mathbf{k}, \tau \rightarrow 0_-)$, we see from Eq. (9) that the amplitude of the mean-field gap is written in the Nambu notation as

$$2\Delta_s = -\frac{g}{\beta} \sum_{\mathbf{k}} \sum_{\omega_n=-\infty}^{\infty} \text{Tr} \left[\tau_1 \eta_2 \overleftrightarrow{G}(\omega_n, \mathbf{k}) \right].$$

Evaluating the trace yields:

$$2\Delta_s = \frac{gv_F \Delta_s}{2\pi v_\Delta} \sum_{\sigma=\pm 1} \int_0^\Lambda d\bar{k} \frac{\bar{k}}{E_{\mathbf{k},\sigma\mu}} \tanh \left(\beta \frac{E_{\mathbf{k},\sigma\mu}}{2} \right) \quad (13)$$

where Λ is a momentum cut-off associated with the linearization of the dispersion close to the CDW nodes.

For $\mu = 0$, the gap equation is rather simple and reads,

$$\Delta_s(T, g, \mu = 0) = \frac{2}{\beta} \cosh^{-1} [\cosh[\pi v_\Delta v_F \beta / g_c] \times e^{-\pi v_\Delta v_F \beta / g}], \quad (14)$$

where $g_c = 2\pi v_\Delta / \Lambda$ is the zero temperature critical coupling constant. In fact,

$$\Delta_s(T = 0, g, \mu = 0) = 2\pi v_\Delta v_F g_c^{-1} \left(1 - \frac{g_c}{g} \right). \quad (15)$$

Notice that for $g < g_c$ we find $\Delta_s(T = 0, g < g_c, \mu = 0) = 0$. Hence, the $\mu = 0$ gap equation has a quantum critical point (QCP), indicating that superconductivity occurs only above a minimal coupling g_c . This is a general property of the nodal liquid due to the absence of the background Fermi sea. In a Fermi liquid (where the

Fermi surface is large in comparison to all the other energy scales), the Fermi sea is unstable to the formation of Cooper pairs between two electrons mediated by an attractive potential, even for infinitesimal coupling³². In this case, the Pauli exclusion principle of the background electrons plays the role of the interaction, making the condensate stable even in the weak coupling limit³³. The zero temperature gap (15) equals to the energy cut-off $\alpha = v_F \Lambda$ in the $g \rightarrow \infty$ limit.

A. Zero temperature analysis

To see how the pocket affects the QCP when $g \sim g_c$ we analyze the gap equation in the zero temperature limit. At this point we introduce a more suitable cut-off, given by the momenta s_\pm that define the surfaces of constant energy in the Dirac cone,

$$\alpha \equiv v_F^2 \Lambda^2 = (v_F s_\pm \pm \mu)^2 + \Delta_s^2 = \text{const.} \quad (16)$$

This new definition of the cut-off (basically replacing Λ by s_σ , with $\sigma = \pm$) is convenient because it simplifies the integration, allowing us to find simple analytical expressions for the gap. This approximation is fairly reasonable, since the results of the model are not to be taken literally when μ and Δ_s are comparable to the energy cut-off of the Dirac cone, α , in which case the contribution of the high energy states cannot be neglected. On the other hand, we should be warned by the fact that this new momentum cut-off s_σ does *not* conserve the number of states of the normal phase. When calculating thermodynamic functions, the correct cut-off is Λ , which correctly maps the volume of the Dirac cone and avoids problems such as loosing states in the SC phase, what would certainly have an effect in the condensation energy. For almost all the applications, the results are not seriously affected by the details of the cut-off if the gap, Δ_s , is sufficiently small in comparison to α .

The $T = 0$ gap equation becomes

$$\begin{aligned} 2\Delta_s &= \frac{gv_F}{v_\Delta} \Delta_s \sum_{\sigma=\pm 1} \int_0^{s_\sigma} \frac{d\bar{k}}{2\pi} \frac{\bar{k}}{E_{\mathbf{k},\sigma\mu}} \\ &= \frac{g}{2\pi v_F v_\Delta} \Delta_s \left[2\alpha - 2\sqrt{\Delta_s^2 + \mu^2} \right. \\ &\quad \left. - \mu \ln \left(\frac{\sqrt{\Delta_s^2 + \mu^2} - \mu}{\sqrt{\Delta_s^2 + \mu^2} + \mu} \right) \right]. \end{aligned} \quad (17)$$

We rescale all the quantities by defining $x = \Delta_s / |\mu|$ and

$$h(g) = 2\pi v_F v_\Delta \frac{g_c^{-1} - g^{-1}}{|\mu|}.$$

The $T = 0$ scale invariant equation is

$$\begin{aligned} F(x, h(g)) &= \sqrt{1+x^2} \\ &\quad + \frac{1}{2} \ln \left(\frac{\sqrt{1+x^2} - 1}{\sqrt{1+x^2} + 1} \right) - h(g) \\ &= 0. \end{aligned} \quad (18)$$

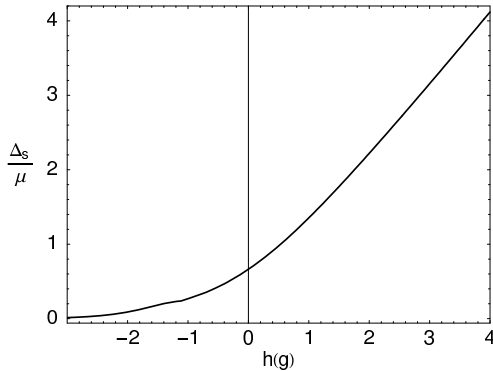


Figure 4: Scaling of the zero temperature gap equation versus the coupling constant $h(g) \propto (g_c^{-1} - g^{-1})/|\mu|$.

We see in Fig. 4 that Eq. (18) has two distinct coupling regimes:

(i) the *strong coupling* sector $g > g_c$, where the marginal physics develops, with $|\mu| \ll \Delta_s(0, g, \mu)$ for $g \gg g_c$;

(ii) the *weak-coupling* sector $g < g_c$, where the energy scale of the pocket is large in comparison to the gap [*i.e.* $|\mu| \gg \Delta_s(0, g, \mu)$] when $g/g_c \rightarrow 0$.

In the later, the system flows in the direction of a Fermi liquid state in the weak-coupling limit ($g \ll g_c$), while in the former the nodes are well defined for $g > g_c$, resulting in a nodal liquid description. We notice that the quasi-particle properties are strongly affected by the coupling constant g , which separates the marginal Fermi liquid (MFL) sector from the “Fermi liquid” one, where the pocket plays the role of the Fermi surface, raising the density of states in the nodes.

For convenience, we denote the zero temperature gap $\Delta_s(0, g, \mu)$ by $\Delta_{0\mu}$ from now on. In the strong coupling limit, ($|\mu|/\Delta_{0\mu} \ll 1$), we may write Eq. (17) as

$$1 = \frac{g}{2\pi v_\Delta v_F} \left(\alpha - \Delta_s + \frac{\mu^2}{2\Delta_s} \right),$$

whose solution is

$$\Delta_{0\mu} \xrightarrow{g \gg g_c} \frac{\Delta_0}{2} \left(1 + \sqrt{1 + 2\mu^2/\Delta_0^2} \right), \quad (19)$$

where $\Delta_0 \equiv \Delta(T = 0, g, \mu = 0)$ is given by Eq. (15). In the opposite limit, $\Delta_{0\mu}/|\mu| \ll 1$, in the weak-coupling sector, we see that Eq. (18) can be expanded in leading order in x , giving

$$\begin{aligned} F(x, h(g)) &\xrightarrow{x \rightarrow 0} 1 + \ln\left(\frac{x}{2}\right) - h(g) \\ &= 1 + \ln\left(\frac{\Delta_s}{2|\mu|}\right) - 2\pi v_F v_\Delta \frac{g_c^{-1} - g^{-1}}{|\mu|} \\ &= 0, \end{aligned}$$

yielding,

$$\begin{aligned} \Delta_{0\mu} &\xrightarrow{g \ll g_c} 2|\mu| e^{h(g, \mu) - 1} \\ &= 2|\mu| e^{2\pi v_F v_\Delta (g_c^{-1} - g^{-1}) |\mu|^{-1} - 1}. \end{aligned} \quad (20)$$

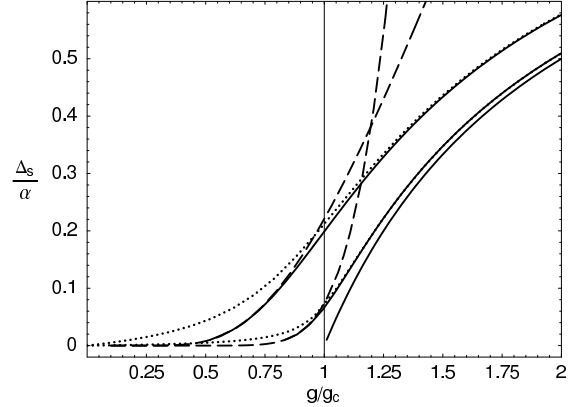


Figure 5: Dependence of the zero temperature gap (normalized by the cut-off α) with the coupling constant g . Solid lines: numeric solution of the gap equation (18); dotted: strong coupling approximation ($|\mu| \ll \Delta_{0\mu}$); dashed: weak coupling one ($|\mu| \gg \Delta_{0\mu}$). We have set $|\mu|/\alpha = 0, 0.1$ e 0.3 from the bottom to the top. Notice that the QCP at $\mu = 0$ is suppressed by the pocket formation ($|\mu| > 0$).

Although the strong coupling approximation is rigorously valid only for $g \gg g_c$, and the weak coupling one for $g \ll g_c$, these two approximations are remarkably good in almost the entire coupling range of their respective sectors (as shown in Fig. 5) provided that $|\mu|/\alpha$ is small. However, to find sensible results, one should consider that the valid coupling range of the theory is limited not too far above the critical coupling g_c , in order to keep the ratio $\Delta_{0\mu}/\alpha$ small (see Fig. 5).

B. Finite temperatures

Let us return to Eq. (13). After some algebraic manipulation (see the details in appendix A), the gap equation in the strong coupling regime assumes the form

$$\begin{aligned} \cosh(\beta\Delta_s/2) e^{-\mu^2\beta \tanh(\beta\Delta_s/2)/(4\Delta_s)} \\ = \cosh(\pi v_\Delta v_F \beta/g_c) e^{-\pi v_\Delta v_F \beta/g}. \end{aligned} \quad (21)$$

The quantity $\tanh(\beta\Delta_s/2)/\Delta_s$ changes very little with β in the whole temperature interval. In a first approximation, we can obtain the analytical expression of the low temperature gap by replacing the gap inside the exponential by its zero temperature value $\Delta_{0\mu}$. This substitution leads to:

$$\begin{aligned} \Delta_s(T, g, \mu) &\sim \frac{2}{\beta} \cosh^{-1} [\cosh(\pi v_\Delta v_F \beta/g_c) \\ &\quad \times e^{-\pi v_\Delta v_F \beta/g} e^{\mu^2\beta \tanh(\beta\Delta_{0\mu}/2)/(4\Delta_{0\mu})}], \end{aligned}$$

valid in strong coupling for small μ/α . Close to the phase transition, Eq. (13) gives

$$\Delta_s(T) \xrightarrow{T \rightarrow T_c} \begin{cases} 2\sqrt{\frac{\Delta_0}{\beta_c} + \frac{\mu^2}{2}} t^{\frac{1}{2}} & , |\mu|/\Delta_{0\mu} \ll 1 \\ \frac{1}{\beta_c} \left[\frac{7\zeta(3)}{8\pi^2} + \frac{1}{2\beta_c^2 \mu^2} \right]^{-\frac{1}{2}} t^{\frac{1}{2}} & , |\mu|/\Delta_{0\mu} \gg 1, \end{cases} \quad (22)$$

where $t \equiv (T_c - T)/T_c$ is the reduced temperature and $\zeta(x)$ is the Zeta function. The critical temperature is also calculated from the gap equation, (13), in the $\Delta_s \rightarrow 0$ limit, giving

$$T_c = \begin{cases} \frac{1}{2k_B \ln 4} \left[\Delta_0 + \sqrt{\Delta_0^2 + \mu^2 \ln 4} \right] & , |\mu|/\Delta_{0\mu} \ll 1 \\ \frac{|\mu|\gamma}{k_B \pi} e^{\alpha(1-g_c/g)|\mu|^{-1}-1} & , |\mu|/\Delta_{0\mu} \gg 1, \end{cases} \quad (23)$$

where $\ln \gamma \sim 0.577$ is the Euler constant. In the particle-hole symmetric case ($\mu = 0$), we have $T_c = \Delta_0/(k_B \ln 4)$ and $\Delta_s(T \rightarrow T_c, g, 0) = 2\Delta_0 t^{\frac{1}{2}}/\ln 2$ (see appendix A for details).

We see that the existence of a pocket suppresses the QCP ($T = 0$) separating the normal and SC phases (see Fig. 5). This effect is due to the establishment of the background Fermi sea, which stabilizes the Cooper pairs for an arbitrarily small coupling. The thermal effect on the gap recovers the parametric phase transition with the coupling constant g , as displayed in Fig. 6 (top) by noting the presence of a minimal coupling (say, $g_0(T, \mu)$, with $g_0(0, 0) = g_c$), below which $\Delta_s(g < g_0, \mu) = 0$. The explanation can be found in the strong dependence of the critical temperature T_c with g , as shown in Fig. 6 (bottom). At a given non-zero temperature T , a minimal coupling is required to satisfy $T_c(g > g_0) > T$.

IV. THERMODYNAMICS

In this section, we calculate the thermodynamic functions starting from the partition function Z of the nodal fermions. The partition function is defined as usual from the original Hamiltonian (8), written in a diagonal basis of eigenstates indexed by \mathbf{k} , $\gamma = \pm 1$ (for the two particle-hole branches), $\sigma = \pm 1$, and with eigenvalues $E_{\mathbf{k}}^a = \pm E_{\mathbf{k},\sigma\mu}$:

$$\begin{aligned} Z &= e^{-\beta\Omega} = \text{tr } e^{-\beta H} \\ &= e^{-\beta g^{-1} \Delta_s^2} \prod_{\mathbf{k}, a} \sum_{n_{\mathbf{k}}^a=0}^1 \langle n_{\mathbf{k}}^a | e^{-\beta E_{\mathbf{k}}^a n_{\mathbf{k}}^a} | n_{\mathbf{k}}^a \rangle \\ &= e^{-\beta g^{-1} \Delta_s^2} \prod_{\mathbf{k}, \gamma, \sigma} (1 + e^{-\beta \gamma E_{\mathbf{k},\sigma\mu}}), \end{aligned}$$

where Ω is the thermodynamic potential. The Hamiltonian includes the term Δ_s^2/g , in order to give the correct condensation energy. The thermodynamic potential,

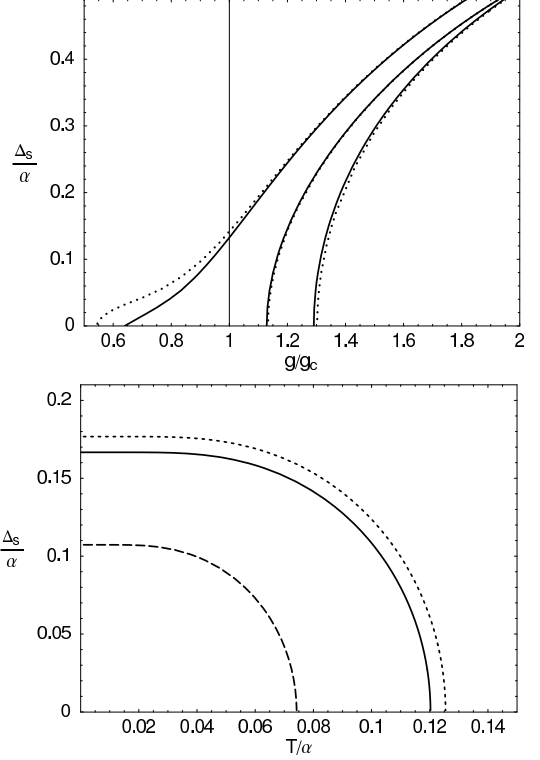


Figure 6: Top: SC gap $\Delta_s(T, g, \mu)$ vs. the coupling constant g/g_c . Solid lines: numeric solution of the gap equation (13); dotted lines: strong coupling solution (analytic). From left to right: $k_B T/\alpha = 0.005, 0.1, 0.2$ and $|\mu|/\alpha = 0.2, 0.1, 0.1$, respectively. Bottom: SC gap vs. temperature. The scales are normalized by the energy cut-off α of the Dirac cone. Dotted line: $(|\mu|/\alpha = 0.06, g/g_c = 1.2)$; solid: $(\mu/\alpha = 0, g/g_c = 1.2)$; dashed: $(|\mu|/\alpha = 0.06, g/g_c = 1.1)$.

$\Omega = \Omega_0 + \Delta_s^2/g$, is given by

$$\begin{aligned} \Omega_0(T) &= -\frac{1}{\beta} \sum_{\mathbf{k}, \sigma} \ln [2 + 2\cosh(\beta E_{\mathbf{k},\sigma\mu})] \\ &= -\frac{v_F}{\pi \beta v_{\Delta}} \sum_{\sigma} \int_0^{\Lambda} d\bar{k} \bar{k} \ln [2 + 2\cosh(\beta E_{\mathbf{k},\sigma\mu})]. \end{aligned} \quad (24)$$

If Ω_n is the thermodynamic potential in the normal phase, the condensation energy, $\Omega_n(0) - \Omega_0(0) = H_c^2(0)/(8\pi)$, is given in terms of the zero temperature critical field, H_c , shown in Fig. 7. Analogously, the internal energy, $E = E_0 + \Delta_s^2/g$, is given by

$$\begin{aligned} E_0(T) &= \sum_{\mathbf{k}, \gamma, \sigma} \gamma E_{\mathbf{k},\sigma\mu} n_{\mathbf{k}}^{\gamma} \\ &= -\frac{v_F}{2\pi v_{\Delta}} \sum_{\sigma} \int_0^{\Lambda} d\bar{k} \bar{k} E_{\mathbf{k},\sigma\mu} \tanh \left(\frac{\beta E_{\mathbf{k},\sigma\mu}}{2} \right). \end{aligned} \quad (25)$$

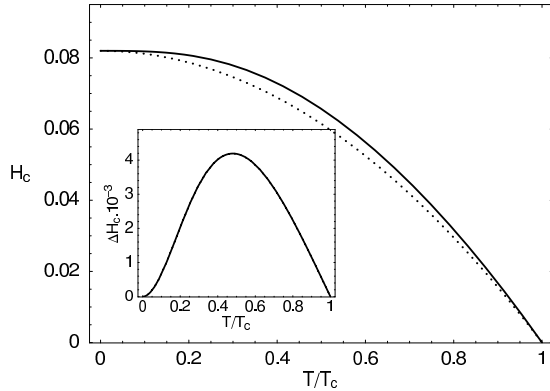


Figure 7: Solid line: critical field H_c dependence with temperature, in units of $\alpha/\sqrt{g_c}$ for $\mu = 0$ and $g/g_c = 1.1$; dotted: empirical law $H_c(0)[1 - T^2/T_c^2]$. The difference between the two curves is shown in the inset.

where $n_{\mathbf{k}}^{\gamma} = (e^{\gamma\beta E_{\mathbf{k},\sigma\mu}} + 1)^{-1}$ is the Fermi-Dirac distribution indexed by $\sigma, \gamma = \pm 1$.

According to the standard thermodynamic relations, the specific heat is defined by

$$C_V = T \frac{dS}{dT} = -\beta \frac{dS}{d\beta}, \quad (26)$$

where $S = (E - \Omega)/T = -(\frac{\partial\Omega}{\partial T})_V$ is the electronic entropy due to the Dirac fermions. At low temperature, the gap is practically independent on the temperature. It is easy to check that the specific heat dependence with temperature in this limit for $\mu = 0$ is given by:

$$\begin{aligned} C_V &\xrightarrow{T \ll T_c} \frac{1}{2\pi v_F v_{\Delta}} \int_{\Delta_s}^{E_{\Delta}} dE E^3 \operatorname{sech}^2\left(\frac{\beta E}{2}\right) \\ &\xrightarrow{\Delta \rightarrow \infty} \frac{6k_B}{\pi v_F v_{\Delta}} \Delta_s^2 e^{-\beta \Delta_s}, \end{aligned}$$

leading to the expected exponential behavior of C_V with the gap.

A more interesting result is related to the jump of the specific heat in the normal-SC phase transition. The calculation is given in appendix B for the weak and strong coupling regimes. It results in two well defined limits: the marginal one ($|\mu/\beta_c| \ll 1$),

$$\left. \frac{\Delta C_V}{C_{n,V}} \right|_{T_c} = \frac{2 \ln 4}{9\zeta(3)} \left(\ln 4 + \frac{\beta_c^2 \mu^2}{2} \right) \geq 0.35,$$

where the equality holds for $\mu = 0$; and the Fermi liquid limit

$$\left. \frac{\Delta C_V}{C_{n,V}} \right|_{T_c} = \frac{3}{2\pi^2} \frac{1}{\frac{7\zeta(3)}{8\pi^2} + \frac{1}{2\beta_c^2 \mu^2}} \leq 1.43, \quad (27)$$

which recovers the BCS result for $\beta_c|\mu| \gg 1$.

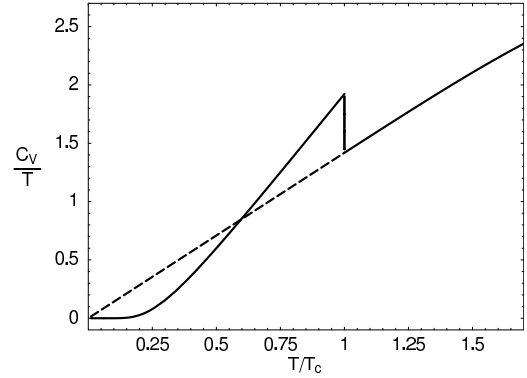


Figure 8: Specific heat C_V/T vs. temperature for $\mu = 0$, in units of k_B^2/g_c . The jump occurs at $k_B T_c = \Delta_0/\ln 4$. Dashed line: normal behavior in the absence of the SC gap.

The jump observed in $\text{NbSe}_2^{34,35,36}$ ($\Delta C/C_n \sim 2$) is a good indication in favor of a conventional Fermi liquid and BCS behavior. In TaSe_2 , however, where the transport is marginal and the quasi-particles are not well defined in the Landau sense³⁷ ($\tau\omega < 1$, where τ^{-1} is the scattering rate), the picture can be very different. In the nodal liquid case, the specific heat jump is strongly attenuated due to the vanishing density of states (DOS) in the Fermi surface, resulting in the universal constant $\Delta C_V/C_n = 0.35$. The plot of the specific heat displayed in Fig. 8 shows that the temperature dependence of the normal CDW phase is quadratic. As the DOS is raised by a pocket around the nodes, the jump grows in direction to the BCS value of 1.43, which corresponds to the weak coupling limit. However, we notice that the nodes cease to be well defined in the presence of large pockets. In this case, the pairing ansatz adopted in sec. II and the role of piezoelectricity in the electron-phonon coupling are questionable.

V. COHERENCE FACTORS

In this section we calculate two basic properties of the superconductor: the acoustic attenuation and the nuclear spin relaxation rate in the absence of impurities.

A. Acoustic attenuation

The ultra-sound attenuation results from the resonant absorption of the longitudinal phonons in the solid³⁸. The absorption rate is proportional to the imaginary part of the charge susceptibility³⁹:

$$\alpha_s(\mathbf{q}) = -\lambda_1^2 \lim_{\omega \rightarrow 0} \left[\frac{1}{\omega} \operatorname{Im} \chi^c(\mathbf{q}, \omega) \right] \quad (28)$$

in the $q \rightarrow 0$ limit, since the phonon wavelength is much larger than the typical electronic wavelength. This prop-

erty is connected to the superconductor *coherence factors*, which basically define the probability amplitude of quasi-particle transitions between two states represented by the pairs space $(\mathbf{k} \uparrow, -\mathbf{k} \downarrow)^{33,38}$. These factors conserve the time reversal symmetries of the interaction involved in the transition. They are usually divided into type I, for interactions which preserve the time-reversal symmetry (like in the electron-phonon coupling) and type II when this symmetry is broken, like in the spin exchange interaction. The charge susceptibility is defined in terms of the time ordered charge density correlation function. All the correlation functions used in this article are defined in appendix C. Using the spinor defined in (7), the charge density operator is given by:

$$\begin{aligned} \rho(\mathbf{q}) &= \sum_{\mathbf{k}, \sigma, a} \psi_{a\sigma}^\dagger(\mathbf{k} - \mathbf{q}/2) \psi_{a\sigma}(\mathbf{k} + \mathbf{q}/2) \\ &= \sum_{\mathbf{k}} \Psi^\dagger(\mathbf{k} - \mathbf{q}/2) \tau_3 \eta_0 \Psi(\mathbf{k} + \mathbf{q}/2). \end{aligned} \quad (29)$$

We define: $\overset{\leftrightarrow}{G}_+ \equiv \overset{\leftrightarrow}{G}(\mathbf{k} + \mathbf{q}/2, i\omega_n + i\omega)$ and $\overset{\leftrightarrow}{G}_- \equiv \overset{\leftrightarrow}{G}(\mathbf{k} - \mathbf{q}/2, i\omega_n)$, so that the electronic charge susceptibility reads

$$\chi^c(\mathbf{q}, i\omega) = \frac{1}{\beta} \text{Tr} \sum_{\mathbf{k}, \omega_n} \overset{\leftrightarrow}{G}_+ \tau_3 \eta_0 \overset{\leftrightarrow}{G}_- \tau_3 \eta_0. \quad (30)$$

It is convenient to define the gapless Dirac fermions dispersion by $\epsilon_{\mathbf{k}} = v_F \bar{k}$, and the quantity $\epsilon_o = \sqrt{v_F^2(\bar{k}^2 + \bar{q}^2)}$. After evaluating the trace and the sum over the fermionic Matsubara frequencies, the imaginary part of the susceptibility reads:

$$\begin{aligned} \text{Im} \chi^c(\mathbf{q}, \omega \rightarrow 0) &= \frac{\omega}{\epsilon_{\mathbf{q}/2}} \frac{v_F}{\pi v_\Delta} \int_0^\Lambda d\bar{k} \bar{k} \sum_{\sigma=\pm 1} \frac{\partial n(E_{o,\sigma\mu})}{\partial E_{o,\sigma\mu}} \\ &\times \frac{\epsilon_o + \sigma\mu}{\epsilon_o E_{o,\sigma\mu}} \sqrt{\epsilon_o^2 - \epsilon_{\mathbf{q}/2}^2}, \end{aligned} \quad (31)$$

where $E_{o,\sigma\mu} = \sqrt{(\epsilon_o + \sigma\mu)^2 + \Delta_s^2}$, and n is the Fermi-Dirac distribution. Replacing Eq. (31) into Eq. (28), we obtain the ultra-sound attenuation rate:

$$\alpha_s \xrightarrow{q \rightarrow 0} -\frac{1}{\epsilon_{\mathbf{q}/2}} \frac{\lambda_1^2}{\pi v_\Delta v_F} \sum_{\sigma=\pm 1} \int_0^\infty \frac{d\epsilon \epsilon}{E_{\sigma\mu}} (\epsilon + \sigma\mu) \frac{\partial n(E_{\sigma\mu})}{\partial E_{\sigma\mu}}.$$

The temperature dependence of α_s is displayed in Fig. 9 and shows a power-law behavior near the phase transition. This result is compared with the BCS curve $\alpha_s/\alpha_n = 2/(e^{\beta\Delta_s} + 1)^{33}$.

B. NMR relaxation

The NMR relaxation has its origin on the hyperfine interaction between the nuclear spins and the electrons. The relaxation rate measures the nuclear spin time-variation along an arbitrary direction of the spin space,

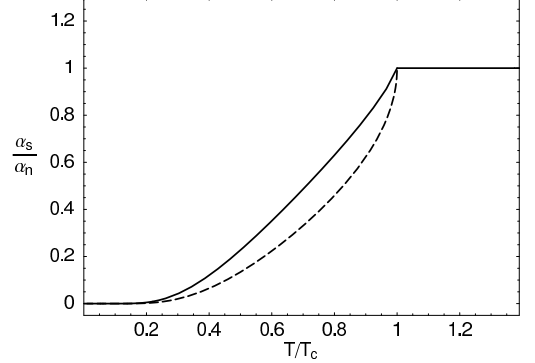


Figure 9: Temperature dependence of the acoustic attenuation rate normalized by the normal phase rate. Solid: our model ($\mu = 0$ and $g/g_c = 1.1$); dashed: BCS model.

say $\hat{\mathbf{b}}$. The condensate exhibits no paramagnetism in the singlet channel, where the total spin of the pairs is zero. Since the Zeeman and hyperfine energies are usually small in comparison to the gap, the only processes that contribute to the spin relaxation are thermally excited quasi-particles. The inverse of the spin relaxation is proportional to the local magnetic susceptibility projected along $\hat{\mathbf{b}}$,

$$T_1^{-1}(\hat{\mathbf{b}}) = -\lambda_2^2 \sum_{\mathbf{q}} \lim_{\omega \rightarrow 0} \left[\frac{1}{\omega} \text{Im} \chi_{\hat{\mathbf{b}}}^s(\mathbf{q}, \omega) \right], \quad (32)$$

where $\chi_{\hat{\mathbf{b}}}^s(\omega)$ is given in terms of the normal directions of the spin space by: $\chi_{\hat{\mathbf{b}}}^s(\omega) = \sum_{ij} (\delta^{ij} - b^i b^j) \chi_{ij}^s(\omega)$, with $i, j = 1, 2, 3$ representing the x, y, z directions, respectively (see appendix C).

Before defining the spin density operator, we must introduce the spin degrees of freedom in the spinor representation, Eq. (7). This is naturally done in the Balian-Werthamer (BW) space⁴⁰,

$$\Psi_a(\mathbf{k}) = \begin{pmatrix} \psi_{a\uparrow}(\mathbf{k}) \\ \zeta_a(\mathbf{k}) \\ -i\sigma_2 \zeta_a^\dagger(-\mathbf{k}) \end{pmatrix} = \begin{pmatrix} \psi_{a\uparrow}(\mathbf{k}) \\ \psi_{a\downarrow}(\mathbf{k}) \\ -\psi_{a\downarrow}^\dagger(-\mathbf{k}) \\ \psi_{a\uparrow}^\dagger(-\mathbf{k}) \end{pmatrix}, \quad (33)$$

which contains an additional spin subspace

$$\zeta(\mathbf{k}) = \begin{pmatrix} \psi_{\uparrow}(\mathbf{k}) \\ \psi_{\downarrow}(\mathbf{k}) \end{pmatrix},$$

inside the regular Nambu space, $(\uparrow \mathbf{k}, \downarrow -\mathbf{k})$. We have defined a new set of Pauli matrices $\sigma_\mu = (\sigma_0, \vec{\sigma})$ which operate in this new space. The general spin density operator is

$$\begin{aligned} S_i(\mathbf{q}) &= \frac{1}{2} \sum_{\mathbf{k}\sigma\sigma' a} \psi_{a\sigma}^\dagger(\mathbf{k} - \mathbf{q}/2) \sigma_i^\sigma \sigma'^{\sigma'} \psi_{a\sigma'}(\mathbf{k} + \mathbf{q}/2) \\ &= \frac{1}{2} \sum_{\mathbf{k} \in \frac{1}{2}\text{B.Z.}} \Psi^\dagger(\mathbf{k} - \mathbf{q}/2) \sigma_i \tau_0 \eta_0 \Psi(\mathbf{k} + \mathbf{q}/2), \end{aligned} \quad (34)$$

where $i = 1, 2, 3$ are the spin directions, \mathbf{k} is summed in half Brillouin zone, and $\sigma, \sigma' = \uparrow\downarrow$ are the spin indexes. It is not difficult to check that the Hamiltonian (8), written in the BW space, is given by (see appendix D)

$$H = \sum_{\mathbf{k} \in \frac{1}{2}\text{B.Z.}} \Psi^\dagger(\mathbf{k}) [v_F \sigma_0 \tau_0 \vec{\eta} \cdot \vec{\mathbf{k}} - \Delta_s \sigma_3 \tau_1 \eta_2 - \mu \sigma_0 \tau_3 \eta_0] \Psi(\mathbf{k}). \quad (35)$$

The matrix inside the parenthesis defines the new dispersion tensor $\vec{\omega}_\mathbf{k}$ for the Green function (12), $\vec{G} = (i\omega_n - \vec{\omega})^{-1}$. Notice that the BW Green function is very similar to the previous one, except for the size of the Hamiltonian space, which now is 8×8 .

The pairing term brings something new, because of the broken time-reversal symmetry of the SC phase, expressed by the anti-symmetric property of the Pauli matrix η_2 under the transposition: $\eta_\alpha^{ab} \rightarrow \eta_\alpha^{ba}$. We will soon explore the physical consequences of this broken symmetry. >From Eq. (C2) the spin susceptibility tensor is given by

$$\chi_{ij}^s(\mathbf{q}, i\omega) = \frac{1}{4\beta} \text{Tr} \sum_{\mathbf{k} \in \frac{1}{2}\text{B.Z.}} \sum_{\omega_n} \vec{G}_+ \sigma_i \tau_0 \eta_0 \vec{G}_- \sigma_j \tau_0 \eta_0. \quad (36)$$

Notice that the product $\sigma_i \tau_0 \eta_0 \vec{G} \sigma_i \tau_0 \eta_0 = \vec{G}$ for $i = 3$. For $i = 1, 2$, the anti-commutative matrices η_i lead to a sign change in the gap term of $\vec{\omega}$ inside the Green function, implying $\Delta_s \rightarrow -\Delta_s$. Thus, the $i = 1, 2$ (i.e. x, y) directions have the same coherence factors of the charge susceptibility,

$$\chi_{xx}^s(\mathbf{q}, \omega) = \chi_{yy}^s(\mathbf{q}, \omega) = \frac{1}{4} \chi^c(\mathbf{q}, \omega). \quad (37)$$

This property is better illustrated in the $\mu = 0$ case, where

$$\chi_{xx}^s = \frac{1}{\beta} \sum_{\mathbf{k}, \omega_n} \frac{(\vec{\epsilon}_- \cdot \vec{\epsilon}_+ - \Delta_s^2) - \omega_n(\omega_n + \omega)}{[\omega_n^2 + E_-^2] [(\omega_n + \omega)^2 + E_+^2]} = \chi_{yy}^s,$$

and

$$\chi_{zz}^s = \frac{1}{\beta} \sum_{\mathbf{k}, \omega_n} \frac{(\vec{\epsilon}_- \cdot \vec{\epsilon}_+ + \Delta_s^2) - \omega_n(\omega_n + \omega)}{[\omega_n^2 + E_-^2] [(\omega_n + \omega)^2 + E_+^2]},$$

with $\vec{\epsilon}_\mathbf{k} \equiv v_F \vec{\mathbf{k}}$, and the indexes \pm representing the momentum, $\pm \rightarrow \mathbf{k} \pm \mathbf{q}/2$. Notice the sign difference in front of Δ_s^2 between the zz and the other two components. This difference gives rise to an axial anisotropy in the z direction of the spin space. This anisotropy is a consequence of the broken time-reversal symmetry induced by the finite momentum of the pairs, \mathbf{Q}_i , which defines the CDW wave vectors. This broken symmetry is reflected in the appearance of a spin structure oriented in the z direction (indicated by the σ_3 matrix) in the pairing term of the BW Hamiltonian (35). Therefore, we conclude that

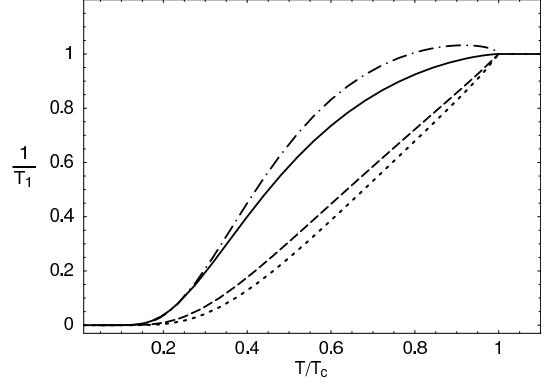


Figure 10: Temperature dependence of the NMR relaxation rate normalized to the normal phase relaxation for $g/g_c = 1.1$. Dashed ($\mu = 0$) and dotted ($|\mu|/\alpha = 0.05$) lines: NMR response along the three CDW directions $\mathbf{b} = \hat{\mathbf{Q}}_i$ ($i = 1, 2, 3$); solid ($\mu = 0$) and dot-dashed ($|\mu|/\alpha = 0.05$) lines: response along the normal directions to the CDW. The pocket produces a small Hebel-Slichter peak, indicated by the dot-dashed line.

the z direction in the spin space corresponds to the CDW direction \mathbf{Q}_i in the k -space, since it is the only rotational symmetry broken in the crystal. The calculation of the imaginary part of the χ_{zz}^s susceptibility reads:

$$\begin{aligned} \text{Im } \chi_{zz}^s(\mathbf{q}, \omega \rightarrow 0) = & \frac{\omega}{4\pi} \frac{v_F}{v_\Delta} \int_0^\Lambda d\bar{k} \bar{k} \\ & \left\{ \frac{\partial n(\tilde{E})}{\partial \tilde{E}} \frac{2\Delta_s^2 \epsilon_{\mathbf{q}/2}^2 - \mu^2}{\tilde{\epsilon}_\mathbf{k} \tilde{E}} \right. \\ & \times \text{Re} \left[\frac{\theta(\tilde{\epsilon}_\mathbf{k} - |\mu|) \tilde{\epsilon}_\mathbf{k} + \theta(|\mu| - \tilde{\epsilon}_\mathbf{k}) |\mu|}{\sqrt{(\epsilon_{\mathbf{q}/2}^2 - \mu^2)(\tilde{\epsilon}_\mathbf{k}^2 - \epsilon_{\mathbf{q}/2}^2)}} \right] \\ & + \sum_{\sigma=\pm 1} \frac{\partial n(E_{o,\sigma\mu})}{\partial E_{o,\sigma\mu}} \frac{E_{o,\sigma\mu}}{(\epsilon_o + \sigma\mu)} \\ & \left. \times \frac{\sqrt{\epsilon_o^2 - \epsilon_{\mathbf{q}/2}^2}}{\epsilon_{\mathbf{q}/2} \epsilon_o} \right\} \end{aligned} \quad (38)$$

where

$$\tilde{\epsilon}_\mathbf{k} = \text{Re} \sqrt{\epsilon_\mathbf{k}^2 + \epsilon_{\mathbf{q}/2}^2 - \mu^2},$$

$\tilde{E}_\mathbf{k} = \sqrt{\tilde{\epsilon}_\mathbf{k}^2 + \Delta_s^2}$ and ϵ_o follows the definition of the previous subsection. The $\chi_{xx,yy}$ can be obtained from the substitution of Eq. (31) into Eq. (37). The NMR relaxation rate along the principal directions gives

$$\frac{1}{T_1}(\hat{b}_i) = \lambda_2^2 \int_0^\Lambda \frac{d\bar{q}}{2\pi} \bar{q} \lim_{\omega \rightarrow 0} \left[\frac{1}{\omega} \left(\text{Im } \chi_{ii}^s - \sum_{j=1}^3 \text{Im } \chi_{jj}^s \right) \right]. \quad (39)$$

In Fig. 10 we distinguish the two anisotropic principal directions $\mathbf{b} = \hat{z}$ and $\mathbf{b} = \hat{x}, \hat{y}$. A small Hebel-Slichter

peak is formed for finite μ , but no peak is observed for $\mu = 0$. The zz component of the susceptibility carries coherence factors with the symmetry of the spin interactions (*i.e.* they are odd by interchanging $\mathbf{k} \rightarrow -\mathbf{k}$), while the xx and yy components are analogous to the charge susceptibility [see Eq. (37)]. This is easily understood by a qualitative argument with the aid of Eq. (39) and Fig. 10. Consider the CDW direction \mathbf{Q}_1 . The \mathbf{Q}_1 direction (or equivalently the $\mathbf{b} = \hat{z}$ direction for the spin, according to our previous discussion) affects the electronic spin correlations in the normal directions to \mathbf{Q}_1 , meaning the xy plane. The NMR direction $\mathbf{b} = \hat{z}$ is affected by the susceptibility components χ_{xx} and χ_{yy} but not by the χ_{zz} one [see Eq. (39)]. The CDW introduces an additional time-reversal broken symmetry to the spin correlations in the \mathbf{Q}_1 (xy) plane, explaining why the related coherence factors have the same symmetry of the charge interactions. Notice from Fig. 10 that the NMR relaxation response in the $\mathbf{b} = z$ direction is very similar to the curve of acoustic attenuation displayed in Fig. 9. On the other hand, the planes which are normal to the \mathbf{Q}_1 plane are affected by the χ_{zz} component, which conserves the odd symmetry of the spin interactions. In summary, the NMR relaxation in the $\hat{\mathbf{b}} = \mathbf{Q}_1$ direction (in k -space) is therefore associated to a *charge-like* symmetry, like in the phonon attenuation response, while the NMR directions which are normal to \mathbf{Q}_1 have a mixed symmetry and exhibit a more intense response, as indicated by Fig. 10. The same analysis applies to the $\mathbf{Q}_{2,3}$ vectors separately. The NMR pattern in the k -space for the SC planes results from the superposition of the contributions due to each vector \mathbf{Q}_i ($i = 1, 2, 3$) of the triple-CDW. As each vector \mathbf{Q}_i is rotated with respect to the other two by $\frac{\pi}{3}$ e $\frac{2\pi}{3}$ (see Fig 1), the anisotropy pattern follows the amplitude dependence of the proposed CDW gap, $|\Delta_c|$, which is maximum along the saddle point directions and minimum in the direction of the nodes. A qualitative picture of the NMR pattern in the SC plane directions is shown in Fig. 11.

VI. TRANSPORT

In this section we calculate the optic and thermal conductivities of the SC phase in the clean limit. The transport calculation for a d -wave order parameter with and without d -wave superconductivity has been done by Yang and Nayak⁴¹. Here, we shall repeat the calculation for a CDW gap with nodes coexisting with a s -wave SC order parameter. We ignore the effects of scattering centers like impurities and disorder from the CDW fluctuations motivated by the two facts: 1) the TMD are very clean materials, and 2) the extremely low temperatures where the SC phase appears in 2H-TaSe₂ ($T \lesssim 0.1$ K), where conventional thermal disorder in the CDW phase should play no relevant role in the transport.

The thermal current is defined by $\mathbf{j}^Q = \mathbf{j}^E - \frac{\mu}{e}\mathbf{j}$,³⁹ where \mathbf{j}^E is the energy current, \mathbf{j} is the electrical current

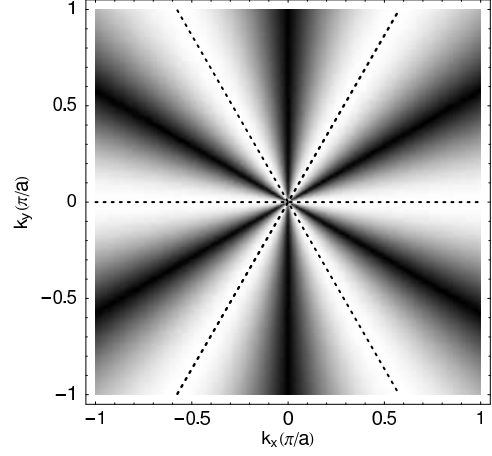


Figure 11: Mapping of the NMR relaxation along the Brillouin zone, with $a \sim \frac{2\pi}{\Lambda}$. Dotted lines: triple-CDW directions \mathbf{Q}_i , $i = 1, 2, 3$. The dark regions represent more intense attenuation directions.

and μ is the chemical potential. Experimental measurements of the thermal conductivity κ require zero electric current flow in the sample, and we may assume that $\mathbf{j}^Q = \mathbf{j}^E$. The Kubo formulas for frequency dependent thermal conductivity, $\kappa(\omega)$, and the optical conductivity, $\sigma(\omega)$, are³⁹:

$$\kappa_{ij}(\omega) = -\frac{1}{\omega T} \lim_{q \rightarrow 0} \text{Im} \Pi_{ij}^{EE}(\mathbf{q}, \omega) + TS_{ij}^2(\omega)\sigma_{ij}(\omega), \quad (40)$$

$$\sigma_{ij}(\omega) = -\frac{1}{\omega} \lim_{q \rightarrow 0} \text{Im} \Pi_{ij}(\mathbf{q}, \omega), \quad (41)$$

where

$$S_{ij}(\omega) = -\frac{1}{T} \lim_{q \rightarrow 0} \left[\frac{\text{Im} \Pi_{ij}^E(\mathbf{q}, \omega)}{\text{Im} \Pi_{ij}(\mathbf{q}, \omega)} \right] \quad (42)$$

is the thermoelectric conductivity (also known as thermopower) $S = -\Delta V/\Delta T$, that measures the current voltage ΔV produced by a temperature gradient ΔT , and Π , Π^{EE} and Π^E are respectively the electric, thermal and thermoelectric current correlation functions, which we define in appendix C. The second term in Eq. (40) guarantees the zero current flow condition to the charge carriers.

A. Optical conductivity

To incorporate the magnetic field into Hamiltonian (8), we proceed with the Peierls substitution $\mathbf{k} \rightarrow \mathbf{k} - \frac{e}{c}\tau_3 \mathbf{A}$. We assume that the vector potential $\mathbf{A}(\mathbf{k})$ is symmetric with respect to momentum inversion in the nodal space. For this reason, we must use the τ_3 Pauli matrix, which operates in the usual Nambu space. Notice

that a given Hamiltonian density for spin $\frac{1}{2}$ fermions in the form $\sum_{\sigma} f(\mathbf{k}) \psi_{\sigma}^{\dagger}(\mathbf{k}) \psi_{\sigma}(\mathbf{k})$ is equivalently written in the Nambu space as

$$\begin{pmatrix} \psi_{\uparrow}^{\dagger}(\mathbf{k}) & \psi_{\downarrow}(-\mathbf{k}) \end{pmatrix} \begin{pmatrix} f(\mathbf{k}) & 0 \\ 0 & -f(-\mathbf{k}) \end{pmatrix} \begin{pmatrix} \psi_{\uparrow}(\mathbf{k}) \\ \psi_{\downarrow}^{\dagger}(-\mathbf{k}) \end{pmatrix}.$$

The associated matrix above is clearly τ_3 if f is a symmetric function in k and τ_0 if f is anti-symmetric. As the Dirac fermion dispersion is anti-symmetric in the cone, we should be especially careful with the usual Peierls substitution, since it introduces an even term ($\propto \tau_3 \mathbf{A}$), which violates the odd symmetry of the zero field dispersion dependence with k . For a given Hamiltonian in the general form:

$$H = \sum_{\mathbf{k}} \epsilon_{\mathbf{k}} \Psi^{\dagger}(\mathbf{k}) \tau_0 \eta_i \Psi(\mathbf{k}),$$

the correct Peierls substitution involves the separation of symmetric (S) and anti-symmetric (A) components in \mathbf{k} ,

$$\epsilon(\mathbf{k}) \tau_0 \rightarrow \epsilon^A(\mathbf{k} - \frac{e}{c} \tau_3 \mathbf{A}) \tau_0 + \epsilon^S(\mathbf{k} - \frac{e}{c} \tau_3 \mathbf{A}) \tau_3, \quad (43)$$

where

$$\begin{aligned} \epsilon^S(\mathbf{k} - \frac{e}{c} \tau_3 \mathbf{A}) &= \frac{1}{2} \left[\epsilon(\mathbf{k} - \frac{e}{c} \tau_3 \mathbf{A}) + \epsilon(-\mathbf{k} - \frac{e}{c} \tau_3 \mathbf{A}) \right], \\ \epsilon^A(\mathbf{k} - \frac{e}{c} \tau_3 \mathbf{A}) &= \frac{1}{2} \left[\epsilon(\mathbf{k} - \frac{e}{c} \tau_3 \mathbf{A}) - \epsilon(-\mathbf{k} - \frac{e}{c} \tau_3 \mathbf{A}) \right]. \end{aligned}$$

Applying this procedure to the Hamiltonian (8), it is easy to see that the magnetic part of the Hamiltonian is

$$H_B = -\Psi^{\dagger}(\mathbf{k}) \left[v_F \frac{e}{c} A_{\perp} \tau_0 \eta_3 + v_{\Delta} \frac{e}{c} A_{\parallel} \tau_0 \eta_1 \right] \Psi(\mathbf{k}),$$

written in terms of τ_0 instead of τ_3 , as one could naively expect from the straight substitution $\mathbf{k} \rightarrow \mathbf{k} - \frac{e}{c} \tau_3 \mathbf{A}$.

The current density operator $\mathbf{j}(\mathbf{k}) = -c \nabla_{\mathbf{A}} H$ is given by

$$\mathbf{j}(\mathbf{k}) = \Psi^{\dagger}(\mathbf{k}) [v_F e \tau_0 \eta_3 \hat{\mathbf{e}}_{\perp} + v_{\Delta} e \tau_0 \eta_1 \hat{\mathbf{e}}_{\parallel}] \Psi(\mathbf{k}). \quad (44)$$

The current-current density correlation function defined in appendix C is given by:

$$\begin{aligned} \Pi_{\perp}(\mathbf{q}, i\omega) &= \frac{v_F^2 e^2}{\beta} \text{Tr} \sum_{\mathbf{k}, \omega_n} \overleftrightarrow{G}_{+} \tau_0 \eta_3 \overleftrightarrow{G}_{-} \tau_0 \eta_3, \\ \Pi_{\parallel}(\mathbf{q}, i\omega) &= \frac{v_{\Delta}^2 e^2}{\beta} \text{Tr} \sum_{\mathbf{k}, \omega_n} \overleftrightarrow{G}_{+} \tau_0 \eta_1 \overleftrightarrow{G}_{-} \tau_0 \eta_1, \end{aligned}$$

where \perp and \parallel are the normal and parallel directions to the Fermi surface for a given node (see Fig. 2). Applying the Kubo formula (41) to the imaginary part of the correlation functions above, we find that the optical conductivity is separated into two parts: the Drude term,

$$\begin{aligned} \sigma_{\perp}^{DC}(\omega) &= -\frac{v_F e^2}{2v_{\Delta}} \delta(\omega) \sum_{\sigma'} \int_0^{\alpha} d\epsilon \epsilon \left(1 - \frac{\Delta_s^2}{E_{\sigma' \mu}^2} \right) \\ &\quad \times \frac{\partial n(E_{\sigma' \mu})}{\partial E_{\sigma' \mu}}, \quad (45) \end{aligned}$$

and an extra term due to the interband excitations of the Dirac fermions,

$$\begin{aligned} \sigma_{\perp}^{AC}(\omega) &= \frac{2v_F e^2}{v_{\Delta}} \frac{\Delta_s^2}{\omega^2} \left[n\left(-\frac{|\omega|}{2}\right) - n\left(\frac{|\omega|}{2}\right) \right] \\ &\quad \times \theta\left(|\omega| - 2\sqrt{\mu^2 + \Delta_s^2}\right) \\ &\quad + \frac{v_F e^2}{2v_{\Delta}} \hbar \omega \nu_0 \left(1 - \frac{4\mu^2}{\omega^2} \right) \\ &\quad \times \left\{ \theta\left(|\mu| - \frac{|\omega|}{2}\right) \frac{1}{\Theta_{-}} [n(E_{0,|\mu|}) - n(E_{0,-|\mu|})] \right. \\ &\quad \left. - \theta\left(\frac{|\omega|}{2} - \sqrt{\mu^2 + \Delta_s^2}\right) \right. \\ &\quad \left. \times \frac{1}{\Theta_{+}} [n(E_{0,\mu}) - n(-E_{0,-\mu})] \right\}, \quad (46) \end{aligned}$$

$$\begin{aligned} &\xrightarrow{T \rightarrow 0} \frac{v_F e^2}{2v_{\Delta}} \left[\left(1 - \frac{4\mu^2}{\omega^2} \right) \frac{\omega \nu_0}{\Theta_{+}} + \frac{4\Delta_0^2}{\omega^2} \right] \\ &\quad \times \theta\left(|\omega| - 2\sqrt{\mu^2 + \Delta_s^2}\right) \end{aligned}$$

where

$$\nu_0 \equiv \frac{\omega}{2} \sqrt{1 - \frac{4\Delta_s^2}{\omega^2 - 4\mu^2}}, \quad (47)$$

and

$$\Theta_{\pm} = |(|\nu_0| - \mu) E_{0,\mu} \pm (|\nu_0| + \mu) E_{0,-\mu}|,$$

with $E_{0,\pm\mu}^2 = (|\nu_0| \pm \mu)^2 + \Delta_s^2$. In order to calculate the the parallel component σ_{\parallel} we just have to replace v_F by v_{Δ} . For $\mu = 0$, the interband conductivity is given by:

$$\sigma_{\perp}^{AC}(\omega) = \frac{e^2 v_F}{2v_{\Delta}} \left(1 + \frac{4\Delta_s^2}{\omega^2} \right) \left| 1 - 2n\left(\frac{\omega}{2}\right) \right| \theta(|\omega| - 2\Delta_s). \quad (48)$$

The conductivity (46) is considerably simpler in the normal CDW phase. Setting the gap Δ_s to zero, we have $\nu_0 \rightarrow \omega/2$ and $E_{0,\pm\mu} \rightarrow \left| \frac{|\omega|}{2} \pm \mu \right|$, leading to:

$$\begin{aligned} \sigma_{\perp CDW}^{AC}(\omega) &= \frac{v_F e^2}{2v_{\Delta}} \left[n\left(-\frac{|\omega|}{2} + \mu\right) - n\left(\frac{|\omega|}{2} + \mu\right) \right] \\ &\xrightarrow{T \rightarrow 0} \frac{v_F e^2}{2v_{\Delta}} \theta\left(\frac{|\omega|}{2} - |\mu|\right). \quad (49) \end{aligned}$$

Analogously, the Drude part of the conductivity becomes

$$\begin{aligned} \sigma_{\perp CDW}^{DC}(\omega) &= \frac{v_F e^2 \beta}{8v_{\Delta}} \delta(\omega) \sum_{\sigma'} \int_0^{\alpha} d\epsilon \epsilon \\ &\quad \times \text{sech}^2 \left(\beta \frac{\epsilon + \sigma' \mu}{2} \right) \\ &\xrightarrow{T \rightarrow 0} \frac{v_F e^2}{2v_{\Delta}} \delta(\omega) \times \begin{cases} \frac{2 \ln(2)}{\beta}, & \text{for } \mu = 0 \\ |\mu|, & \text{for } \mu \neq 0. \end{cases} \quad (50) \end{aligned}$$

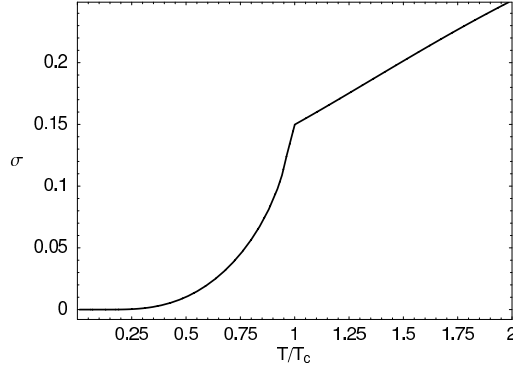


Figure 12: Temperature dependence of the Drude conductivity integrated in ω , for $g/g_c = 1.1$ and $\mu/\alpha = 0.1$. σ in units of $v_F e^2 \alpha / (2v_\Delta)$.

Notice that in the absence of SC we find that $\sigma^{DC}(T \rightarrow 0)$ is constant and proportional to μ . In the SC case, Eq. (45) shows that $\sigma^{DC}(T \rightarrow 0)$ vanishes independently of the pocket size (as shown in Fig. 12). The presence of a Drude conductivity, $\sigma^{DC} \propto \delta(\omega)$, results from an infinite electron mean free path due to the absence of scattering centers. If we consider that the electrons in TaSe₂ have a finite scattering rate, $\Gamma = 1/\tau(\omega)$ ³⁷, the Drude peak will be broadened around $\omega = 0$. The normal transport in the presence of an order parameter with nodes (like the CDW, as in our case) in the dirty limit, is given in Ref. [41].

Photon absorption involves quasiparticle excitations and results in the formation of in-phase currents with the electric field⁴². The absorption rate is therefore proportional to the real part of the conductivity. In conventional superconductors there is no absorption at $T = 0$ in the infrared region where the photons with energy $\omega < 2\Delta_s$ cannot break a Cooper pair. At finite temperature, the excitation channels are gradually recovered and photons with energy smaller than $2\Delta_s$ have a finite probability of being absorbed. We should stress that the coherence factors in those superconductors (say, BCS type) are finite only in the dirty case, where the processes conserve energy but do not conserve momentum. The first important distinction between traditional BCS superconductors to the ones discussed here is the presence of *two* bands, resembling the spectrum of small gap semiconductors (see Fig. 3). In the nodal liquid superconductor, made out of Cooper pairs of Dirac fermions, the absorption process comprehends the excitation of an electron from the lower to the upper band, transferring energy equal to the the photon energy ω but with no momentum transfer. In the situation where the lower band is completely filled ($\mu = 0$), there are no thermal channels of quasiparticle excitations (since the thermally excited electrons occupy the upper band, where there is no absorption due to momentum conservation) and the photon is absorbed only when its energy is sufficient to break a pair ($|\omega| > 2\Delta_s$),

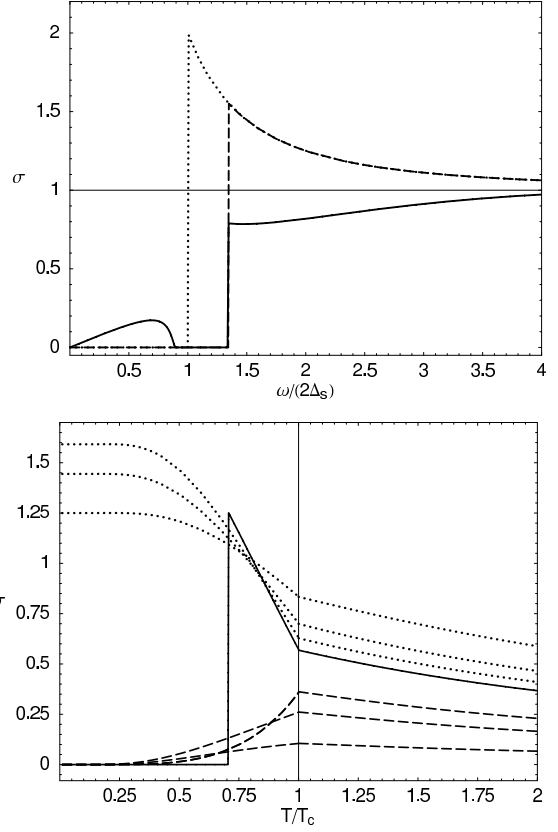


Figure 13: Top: optical conductivity σ_\perp vs. frequency. For $|\mu|/(2\Delta_s) = 0.9$: dashed line ($T = 0$) and solid ($k_B T/(2\Delta_s) = 1.2$); dotted line: $\mu = 0$ and $T = 0$. Bottom: optical conductivity σ_\perp vs. temperature, for $g/g_c = 1.1$ and $|\mu|/\alpha = 0.1$. Dashed lines: $0.4\Delta_{0\mu} < \omega < 1.4\Delta_{0\mu}$; solid: $\omega = 2.3\Delta_{0\mu}$; dotted: $2.8\Delta_{0\mu} < \omega < 4\Delta_{0\mu}$. In both plots, σ is in units of $v_F e^2 / (2v_\Delta)$

producing quasiparticle excitations directly from the condensate (pair breaking channels). When the system exhibits particle-hole symmetry, the absorption is independent of the temperature in the infrared for $\omega < 2\Delta_s$.

The second important distinction between the TMD and BCS superconductors, is that the optical conductivity shows an anomalous absorption edge in $\omega = 2\sqrt{\mu^2 + \Delta_s^2}$ (see Fig. 13). This energy corresponds to the optical gap of the two bands shown in Fig. 3. The presence of the edge is a consequence of the broken lattice inversion symmetry in the CDW phase, which affects the coherence factors of the infrared conductivity. When the particle-hole symmetry is lost by shifting the chemical potential from the vertex of the Dirac cone, new thermal channels of quasiparticle excitations emerge, giving rise to an absorption peak in the infrared. To see this effect, we illustrate in Fig. 14 the thermal excitation process of the hole-like branch, where the photons with energy smaller than $2|\mu|$ are able to promote the thermally excited electrons occupying the empty states on

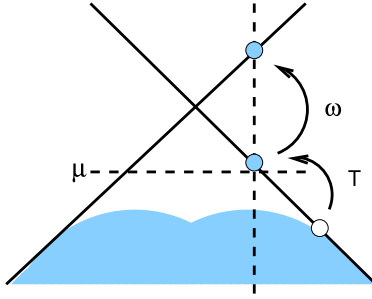


Figure 14: Schematic representation of the photon absorption process in the channel of thermal excitations of the condensate, within the absorption window $|\omega| < 2|\mu|$ of the hole-like branch (see Fig. 3). ω is the photon frequency, T represents the thermal excitations and μ indicates the Fermi level.

the top of the lower band to the upper band. As in the case of superfluid He^3 , the superconductor is an electronic liquid composed of two “fluids”, where there is a one-to-one correspondence between the excited states in the SC and in the normal phases. The thermal fluctuations promote electrons from the condensate to the empty states above the pocket Fermi surface of the hole-like branch. The optical channels of absorption through the thermally excited electrons are therefore limited to the window $|\omega| \leq 2|\mu|$ (in the clean limit), as shown in Fig. 13 (top) and Fig. 14.

The temperature dependence of the optical conductivity, displayed in Fig. 13 (bottom), shows a clear distinction between the two absorption channels. The dashed lines represent the thermal channels, which vanish at $T = 0$. The dotted lines indicate the pair breaking channels. These channels depend on the number of electrons in the condensate and are more effective as the temperature is reduced. The solid line in the same figure represents a pair breaking channel which is abruptly suppressed by lowering the temperature. This is understood by noting that the optical gap $2\sqrt{\mu^2 + \Delta_s^2(T)}$ [see Fig. 13 (top)] displaces the absorption edge towards the ultraviolet as the temperature is reduced. In this situation, we expect that some of the absorption channels, at a given energy slightly to the right of the edge, will be abruptly suppressed if the temperature is sufficiently reduced, *i.e.* if the edge is sufficiently displaced to the right in Fig. 13.

1. Spectral weight

According to the f -sum rule one should have

$$\int_0^\infty \sigma(\omega) d\omega = \frac{\pi n e^2}{2m}, \quad (51)$$

and therefore, the area “under” the curves $\sigma_s^{DC} + \sigma_s^{AC}$ is conserved in the normal and in the SC phases. In the SC

phase, however, there is a “missing” area in comparison to the normal phase. The difference between the two areas corresponds to the $\omega = 0$ spectral weight, responsible for the diamagnetic supercurrents in the Meissner effect³³. This part of the spectral weight (which properly defines a superconductor) depends on a different order of limits between ω and q , and does not appear explicitly in the calculation. Thus, a required condition for superconductivity is

$$\int_0^\infty [\sigma_s^{DC}(\omega) + \sigma_s^{AC}(\omega)] d\omega < \int_0^\infty [\sigma_n^{DC}(\omega) + \sigma_n^{AC}(\omega)] d\omega.$$

>From now on, we call the difference between the n and s areas as the *Meissner spectral weight*.

It is not difficult to see that for $\mu = 0$ at zero temperature we have $\sigma_s^{DC} = \sigma_n^{DC} = 0$, and that the curves in the AC sector have *exactly* the same area. This behavior is depicted in Fig. 15 for different values of μ , showing an anomalous suppression of the Meissner spectral weight at low temperatures for small μ . A superficial analysis would indicate that there is no spectral weight due to the condensate and therefore the superconductivity is not stable. This analysis, however, is incompatible with the thermodynamic verification that there is a finite zero temperature critical field $H_c(0)$ (see Fig. 7), resulting in a finite condensation energy. The origin of the problem has connections with the spectral weight shift from the high to the low energy states of the band as the temperature is reduced, which has been observed experimentally in TaSe_2 ²². In this compound, part of the spectral weight around 60 meV (\sim of the order of the cone cut-off) at 300 K is displaced towards the infrared at temperatures of the order of the SC phase transition. Apparently, the opening of the gap “attracts states” beyond the cone approximation. In the lowest order, the non-linear states in the CDW spectrum yield $\epsilon_{\mathbf{k}} \propto (k - \frac{e}{c}A)^2$. These states are the only ones that contribute to the diamagnetism, which results from terms $\propto A^2$ in the energy. We conclude that the cone approximation excludes the “diamagnetic” states of the band, and for this reason the f -sum rule is not able to correctly incorporate the diamagnetic spectral weight, specially at low temperature, where the contribution of the high energy states is more pronounced. The zero field properties which are not directly related to the Meissner effect, however, are not so sensitive to the absence of the high energy states and give satisfactory results within the cone approximation. This analysis is confirmed later in sec. VII, when we discuss the Meissner effect in the London limit.

B. Thermal conductivity

The energy current is a conserved quantity defined by the non-diagonal components of the momentum-energy

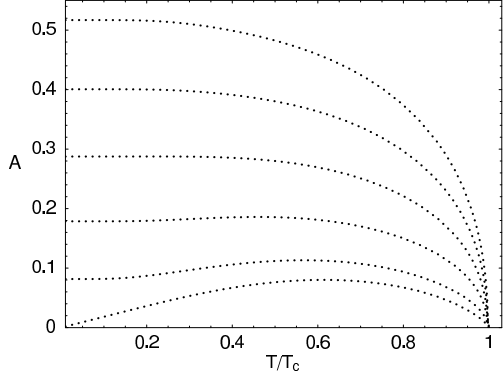


Figure 15: Meissner spectral weight A as a function of temperature. Curves drawn for $0 \leq |\mu|/\alpha \leq 0.15$, from the bottom to the top, in fixed intervals of 0.03. A in units of $v_F e^2 \alpha / (2v_\Delta)$, with $g/g_c = 1.1$.

tensor T_0^i , defined as⁴³

$$T_\nu^\mu \equiv \frac{\partial \mathcal{L}}{\partial(\partial_\mu \Psi)} \partial_\nu \Psi - \mathcal{L} \delta_\nu^\mu. \quad (52)$$

According to the usual relation $H = \frac{\partial \mathcal{L}}{\partial(\partial_0 \Psi)} \partial_0 \Psi - \mathcal{L}$, the Lagrangian associated to the Hamiltonian (8) in the real space representation is

$$\mathcal{L} = \Psi^\dagger(x) [ic\tau_3 \eta_0 \partial_0 - i\hbar v_F \tau_0 \eta_3 \partial_3 - iv_\Delta \tau_0 \eta_1 \partial_1 - \Delta_s \tau_1 \eta_2 + \mu \tau_3 \eta_0] \Psi(x), \quad (53)$$

where $c\partial_0 \equiv i\partial_\tau$ with τ as the imaginary time. The conserved energy current $\mathbf{j}^E(x) = cT_0^i$ gives

$$\begin{aligned} \mathbf{j}^E(x) &= \frac{\partial \mathcal{L}}{\partial(\partial_i \Psi)} c\partial_0 \Psi \\ &= \Psi^\dagger(x) [v_F \tau_0 \eta_3 \hat{\mathbf{e}}_\perp + v_\Delta \tau_0 \eta_1 \hat{\mathbf{e}}_\parallel] \partial_\tau \Psi(x), \end{aligned}$$

or equivalently

$$\begin{aligned} \mathbf{j}^E(\mathbf{q}, \tau) &= - \sum_{\mathbf{k}} \Psi^\dagger(\mathbf{k} - \mathbf{q}/2, \tau) [v_F \tau_0 \eta_3 \hat{\mathbf{e}}_\perp \\ &\quad + v_\Delta \tau_0 \eta_1 \hat{\mathbf{e}}_\parallel] \overleftrightarrow{\omega}_{\mathbf{k}+\mathbf{q}/2} \Psi(\mathbf{k} + \mathbf{q}/2, \tau), \end{aligned} \quad (54)$$

where the time-evolution of the Dirac fermions Ψ is

$$\Psi(\mathbf{q}, \tau) = e^{-\tau \overleftrightarrow{\omega}(\mathbf{q})} \Psi(\mathbf{q}),$$

with $\overleftrightarrow{\omega}$ defined in Eq. (8).

We are interested in the diagonal components of the current-current polarizations $\Pi_{11}^{EE} \equiv \Pi_\perp^{EE}$ and $\Pi_{11}^E \equiv \Pi_\perp^E$ given by:

$$\begin{aligned} \Pi_\perp^{EE}(\mathbf{q}, i\omega) &= \frac{v_F^2}{\beta} \text{Tr} \sum_{\mathbf{k}, \omega_n} \overleftrightarrow{G}_+ \tau_0 \eta_3 \overleftrightarrow{\omega}_+ \overleftrightarrow{G}_- \tau_0 \eta_3 \overleftrightarrow{\omega}_-, \\ \Pi_\perp^E(\mathbf{q}, i\omega) &= \frac{v_F^2 e}{\beta} \text{Tr} \sum_{\mathbf{k}, \omega_n} \overleftrightarrow{G}_+ \tau_0 \eta_3 \overleftrightarrow{\omega}_+ \overleftrightarrow{G}_- \tau_0 \eta_3. \end{aligned}$$

We find that

$$\begin{aligned} \text{Im} \Pi_\perp^{EE}(0, \omega) &= \frac{v_F \omega}{2v_\Delta} \delta(\omega) \sum_{\sigma'=\pm 1} \int_0^\alpha d\epsilon \epsilon E_{\sigma' \mu}^2 \\ &\quad \times \left(1 - \frac{\Delta_s^2}{E_{\sigma' \mu}^2} \right) \frac{\partial n(E_{\sigma' \mu})}{\partial E_{\sigma' \mu}} \\ &\quad - \frac{v_F}{2v_\Delta} \omega^2 \nu_0 \left(1 - \frac{4\mu^2}{\omega^2} \right) E_{0, \mu} E_{0, -\mu} \\ &\quad \times \left\{ \theta\left(|\mu| - \frac{|\omega|}{2}\right) \frac{1}{\Theta_-} [n(E_{0, |\mu|}) - n(E_{0, -|\mu|})] \right. \\ &\quad \left. + \theta\left(\frac{|\omega|}{2} - \sqrt{\mu^2 + \Delta_s^2}\right) \right. \\ &\quad \left. \times \frac{1}{\Theta_+} [n(E_{0, \mu}) - n(-E_{0, -\mu})] \right\} \\ &\quad + \frac{v_F \omega}{2v_\Delta} \Delta_s^2 \left[n\left(-\frac{|\omega|}{2}\right) - n\left(\frac{|\omega|}{2}\right) \right] \\ &\quad \times \theta\left(|\omega| - 2\sqrt{\mu^2 + \Delta_s^2}\right), \end{aligned} \quad (55)$$

and

$$\begin{aligned} \text{Im} \Pi_\perp^E(0, \omega) &= \frac{v_F e}{4v_\Delta} \omega^2 |\nu_0| \left(1 - \frac{4\mu^2}{\omega^2} \right) \\ &\quad \times \left\{ \theta\left(|\mu| - \frac{|\omega|}{2}\right) [E_{0, \mu} - E_{0, -\mu}] \right. \\ &\quad \left. \times \frac{1}{\Theta_-} [n(E_{0, \mu}) - n(E_{0, -\mu})] \right\} \\ &\quad - \theta\left(\frac{|\omega|}{2} - \sqrt{\mu^2 + \Delta_s^2}\right) [E_{0, \mu} + E_{0, -\mu}] \\ &\quad \times \frac{1}{\Theta_+} [n(E_{0, \mu}) - n(-E_{0, -\mu})] \} \\ &\quad + \frac{v_F e}{v_\Delta} \Delta_s^2 \left[n\left(-\frac{|\omega|}{2}\right) - n\left(\frac{|\omega|}{2}\right) \right] \\ &\quad \times \theta\left(|\omega| - 2\sqrt{\mu^2 + \Delta_s^2}\right). \end{aligned} \quad (56)$$

In contrast with the thermal polarization, the thermoelectric one does not have a Drude part. The thermal conductivity follows from a straightforward substitution of the previous results (46), (55) and (56) into the Kubo formula (40).

Let us analyze these results for $\mu = 0$. We have

$$\begin{aligned} \frac{1}{\omega} \text{Im} \Pi_\perp^{EE}(0, \omega) &= \frac{v_F}{v_\Delta} \delta(\omega) \int_{\Delta_s}^{E_\Lambda} dE^3 \left(1 - \frac{\Delta_s^2}{E^2} \right) \\ &\quad \times \frac{\partial n(E)}{\partial E} \\ &\quad + \frac{v_F}{2v_\Delta} \left(\frac{\omega}{2} \right)^2 \left(1 + \frac{4\Delta_s^2}{\omega^2} \right) \\ &\quad \times \left[1 - 2n\left(\frac{|\omega|}{2}\right) \right] \theta(\omega - 2\Delta_s), \end{aligned} \quad (57)$$

and

$$\frac{1}{\omega} \text{Im} \Pi_{\perp}^E(0, \omega) = \frac{ev_F}{2v_{\Delta}} \frac{\omega}{2} \left(1 + \frac{4\Delta_s^2}{\omega^2} \right) \times \left[1 - 2n\left(\frac{\omega}{2}\right) \right] \theta(|\omega| - 2\Delta_s). \quad (58)$$

Replacing Eq. (48) and (58) into Eq. (42), the $\mu = 0$ thermopower yields

$$S_{\perp} = -\frac{1}{T} \frac{\text{Im} \Pi_{\perp}^E(0, \omega)}{\text{Im} \Pi_{\perp}(0, \omega)} = \frac{\omega}{2eT}. \quad (59)$$

Substituting Eq. (48), (57) and (59) into (40), we find that the only contribution comes from the Drude term

$$\kappa_{\perp}(\omega) = -\frac{v_F}{v_{\Delta}T} \delta(\omega) \int_{\Delta_s}^{E_{\Lambda}} dE E^3 \left(1 - \frac{\Delta_s^2}{E^2} \right) \frac{\partial n(E)}{\partial E}, \quad (60)$$

where $\kappa^{AC} = 0$ for zero μ . When the system exhibits particle-hole symmetry, the exact cancellation of the interband contributions to the thermal conductivity is due to the fact that the total heat carried by a particle-hole pair is zero. The argument is the following⁴¹: the interband excitation process involves the annihilation of an electron with negative energy in the lower band, and the creation of a particle with positive energy $-E_{\mathbf{k}} + \omega = +E_{\mathbf{k}}$ in the upper band, where ω is the photon energy and $-E_{\mathbf{k}}$ is the energy of the annihilated electron. Destroying a particle with negative energy, momentum \mathbf{k} and charge e is equivalent to create a hole with momentum $-\mathbf{k}$ and charge $-e$ at the energy cost $+E_{\mathbf{k}}$. The energy current carried by the quasiparticle formed by the particle-hole pair is $\mathbf{k} E_{\mathbf{k}} + (-\mathbf{k})(E_{\mathbf{k}}) = 0$. On the other hand, the charge current is finite, $\mathbf{k} e + (-\mathbf{k})(-e) = 2e\mathbf{k}$, explaining why the quasiparticles are able to transport charge but not heat when the pocket is absent.

When the particle-hole symmetry symmetry is lost, the thermal current due to the pair breaking channels is equal to $E_{\mathbf{k},-\mu}(\mathbf{k}) + (E_{\mathbf{k},\mu})(-\mathbf{k})$, or equivalently to $-2\mu\mathbf{k}$ in the normal CDW phase, when the ground state electrons are promoted to the upper band. As a second effect, the thermal channels of quasiparticle production give rise to an infrared peak for $|\omega| < 2|\mu|$ as shown in Fig. 16 (top), analogously to the optical conductivity. In contrast with the charge transport, however, the amount of heat carried by the quasiparticles is of the order of the pocket energy and vanishes at $\mu = 0$. The temperature dependence of κ is shown in Fig. 16 (bottom). The solid lines represent the thermal channels of quasiparticle excitation, while the dotted lines indicate the pair breaking channels. As in case of the optical conductivity, some of the latter channels which are slightly above the optical gap energy $\omega_0 = 2\sqrt{\mu^2 + \Delta_s^2}$ are suppressed at low temperatures (see Fig. 16). At $T = 0$ the thermal conductivity is zero for $|\omega| < \omega_0$, and infinity for $|\omega| > \omega_0$.

Let us verify the normal CDW properties ($\Delta_s = 0$) in the transport. The thermoelectric spectral function (56)

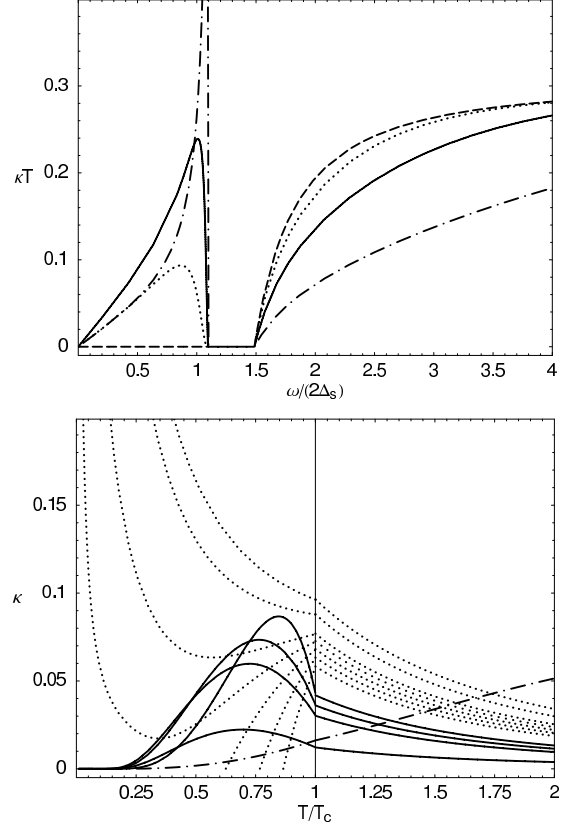


Figure 16: Top: thermal conductivity $\times T$ vs. frequency. κT is in units of $(2v_F/v_{\Delta})\Delta_s^2$ and ω in units of $2\Delta_s$, with $\mu = 2.2\Delta_s$. Dashed line: $T \rightarrow 0$ limit; dotted ($k_B T = \frac{1}{2}\Delta_s$); solid: ($k_B T = \Delta_s$); dot-dashed: ($k_B T = \frac{5}{2}\Delta_s$). Below: thermal conductivity dependency with temperature. We have set κ in units of $v_F k_B \alpha/(2v_{\Delta})$, $g/g_c = 1.1$ and $|\mu/\alpha| = 0.1$. Solid lines: $0.4\Delta_{0\mu} < \omega < 1.4\Delta_{0\mu}$; dotted: $2\Delta_{0\mu} < \omega < 4\Delta_{0\mu}$. The dot-dashed line is the Drude thermal conductivity integrated in ω , with units of $\frac{1}{5}v_F k_B \alpha^2/(2v_{\Delta})$.

is given by

$$\frac{1}{\omega} \text{Im} \Pi_{\perp CDW}^E(0, \omega) = \frac{v_F e}{2v_{\Delta}} \frac{\omega}{2} \left[n\left(-\frac{|\omega|}{2} + \mu\right) - n\left(\frac{|\omega|}{2} + \mu\right) \right].$$

Comparing the expression above with the optical conductivity of the normal phase (49), the thermoelectric coefficient yields

$$S_{\perp CDW}(\omega) = \frac{\omega}{2eT},$$

as in the SC particle-hole symmetric case (59). Returning

to Eq. (55), and setting $\Delta_s = 0$, we have

$$\frac{1}{\omega} \text{Im} \Pi_{\perp CDW}^{EE}(0, \omega) = \frac{v_F}{2v_\Delta} \left[\left(\frac{\omega}{2} \right)^2 - \mu^2 \right] \times \left[n \left(-\frac{|\omega|}{2} + \mu \right) - n \left(\frac{|\omega|}{2} + \mu \right) \right].$$

The thermal conductivity is given by:

$$\kappa_{CDW}(\omega) = \kappa_{CDW}^{DC}(\omega) + \kappa_{CDW}^{AC}(\omega),$$

where

$$\begin{aligned} \kappa_{\perp CDW}^{DC}(\omega) &= -\frac{v_F \delta(\omega)}{2v_\Delta T} \sum_{\sigma'=\pm 1} \int_0^\alpha d\epsilon \epsilon E_{\sigma' \mu}^2 \\ &\quad \times \frac{\partial n(E_{\sigma' \mu})}{\partial E_{\sigma' \mu}} \\ &\xrightarrow{T \rightarrow 0} \frac{v_F k_B}{2v_\Delta \beta^2} \delta(\omega) \times \begin{cases} 9\zeta(3) & \text{, for } \mu = 0 \\ \frac{\pi^2}{3} \beta |\mu| & \text{, for } \mu \neq 0, \end{cases} \end{aligned} \quad (61)$$

and

$$\begin{aligned} \kappa_{\perp CDW}^{AC}(\omega) &= \mu^2 \frac{v_F}{2v_\Delta T} \left[n \left(-\frac{|\omega|}{2} + \mu \right) - n \left(\frac{|\omega|}{2} + \mu \right) \right] \\ &\xrightarrow{T \rightarrow 0} \mu^2 \frac{v_F}{2v_\Delta T} \theta \left(\frac{|\omega|}{2} - |\mu| \right). \end{aligned} \quad (62)$$

The verification of the Wiedmann-Franz (WF) law can be done in two cases. For $\mu = 0$, despite the optical conductivity is dominated in the low temperature region by the interband conductivity,

$$\begin{aligned} \sigma_{\perp CDW}(\omega, T \rightarrow 0) &= \frac{v_F e^2}{2v_\Delta} \tanh \left(\frac{\beta \omega}{4} \right) \\ &\quad + \ln(2) \frac{v_F e^2}{v_\Delta \beta} \delta(\omega), \end{aligned} \quad (63)$$

the $\omega/(k_B T) \ll 1$ limit is dominated by the Drude part. Comparing the expression above with Eq. (61) for $\mu = 0$, we see that the CDW phase obeys the temperature dependence of the WF law

$$\lim_{T \rightarrow 0} \frac{\kappa_{CDW}(0, T)}{T \sigma_{CDW}(0, T)} = \frac{9\zeta(3)}{2 \ln(2)} \left(\frac{k_B}{e} \right)^2, \quad (64)$$

but with a particular numerical constant $9\zeta(3)/(2 \ln(2)) \approx 7.8$. Note that the order of the limits is essential, otherwise, σ_{CDW} is dominated by the interband term in the $\omega/(k_B T) \gg 1$ limit,

$$\lim_{\omega \rightarrow 0} \sigma_{CDW}(\omega, 0) = \frac{v_F e^2}{2v_\Delta},$$

violating the WF law. We should stress, however that this relation is typically valid in the DC limit $\omega \rightarrow 0$, which is well defined for $\beta \omega \ll 1$ but not for $\beta \omega \gg 1$. This is easily seen by noticing that at $T = 0$ the quasi-particle excitation energy ω do not have a scale and the

AC and DC sectors cannot be distinguished. For finite μ , it is immediate to check that the WF relation is verified exactly as in a metal,

$$\lim_{T \rightarrow 0} \frac{\kappa_{CDW}(0, T)}{T \sigma_{CDW}(0, T)} = \frac{\pi^2}{3} \left(\frac{k_B}{e} \right)^2,$$

irrespectively of the order of the T, ω limits.

VII. MEISSNER EFFECT

The non-local electrodynamics is described in the London limit, where the vector potential function $\mathbf{A}(\mathbf{k}) \rightarrow \mathbf{A}_0 = \text{const.}$ under the assumption that the field variations are slow in comparison to the coherence length ξ . In this limit, the current \mathbf{j} and the vector potential obey the London equation

$$\langle j_i \rangle = j_i^{CM} + Q_{ij} A_j,$$

valid in the Coulomb gauge $\mathbf{k} \cdot \mathbf{A} = 0$, where \mathbf{j}^{CM} is the current due to the momentum of the pair center of mass. For all purposes, we neglect this effect and consider only the response to the magnetic field.

In order to calculate the London kernel Q_{ij} , instead of writing the current density operator (44), we propose a more general procedure, extending the CDW band beyond the cone approximation. As in sec. II, we start from a CDW Hamiltonian written in terms of an extended band

$$H_{CDW} = \sum_{\mathbf{k}, \sigma} \Psi_\sigma^\dagger(\mathbf{k}) [\epsilon_\mathbf{k} \eta_3 + \Delta_c \eta_1] \Psi_\sigma(\mathbf{k}), \quad (65)$$

where $\epsilon_\mathbf{k}$ and $\Delta_c \mathbf{k}$ are *any* anti-symmetric k -functions with respect to a given Fermi surface node.

Introducing the magnetic field through the modified Peierls substitution (43), the series expansion of $\epsilon(\mathbf{k} - \frac{e}{c} \tau_3 \mathbf{A})$ in powers of \mathbf{A} is separated into symmetric and anti-symmetric terms in k ,

$$\begin{aligned} \epsilon(\mathbf{k} - \frac{e}{c} \tau_3 \mathbf{A}) &= [\epsilon^{(0)}(\mathbf{k}) + \epsilon^{(2)}(\mathbf{k}) + \dots] \tau_0 + \\ &\quad [\epsilon^{(1)}(\mathbf{k}) + \epsilon^{(3)}(\mathbf{k}) + \dots] \tau_3 \\ &= [\epsilon_\mathbf{k} - \frac{e}{c} A_i \partial^i \epsilon_\mathbf{k} + \frac{1}{2} \left(\frac{e}{c} \right)^2 A_i A_j \partial^i \partial^j \epsilon_\mathbf{k}] \tau_0, \end{aligned}$$

up to second order in \mathbf{A} , where $\partial^i \equiv \frac{\partial}{\partial k_i}$ defines the momentum derivatives and repeated indexes are to be summed. The same applies to $\Delta_c(\mathbf{k} - \frac{e}{c} \tau_3 \mathbf{A})$. Using the abbreviation $\tilde{\mathbf{k}} \equiv \mathbf{k} - \frac{e}{c} \tau_3 \mathbf{A}$, the Hamiltonian of the CDW + SC phase with an external magnetic field is

$$\begin{aligned} H &= \sum_{\mathbf{k}} \Psi^\dagger(\tilde{\mathbf{k}}) [\epsilon_{\tilde{\mathbf{k}}} \tau_0 \eta_3 + \Delta_{c\tilde{\mathbf{k}}} \tau_0 \eta_1 \\ &\quad + \Delta_s \tau_1 \eta_2 - \mu \tau_3 \eta_0] \Psi(\tilde{\mathbf{k}}). \end{aligned}$$

The current density operator $\overset{\leftrightarrow}{j}_i(\mathbf{k}) = -c\nabla_{\mathbf{A}}H$ gives

$$\begin{aligned}\overset{\leftrightarrow}{j}_i(\mathbf{k}) &= \Psi^\dagger(\tilde{\mathbf{k}}) \left[e \left(\partial^i \epsilon_{\mathbf{k}} - \frac{e}{c} A_j \partial^i \partial^j \epsilon_{\mathbf{k}} \right) \tau_0 \eta_3 \right. \\ &\quad \left. + e \left(\partial^i \Delta_{c\mathbf{k}} - \frac{e}{c} A_j \partial^i \partial^j \Delta_{c\mathbf{k}} \right) \tau_0 \eta_1 \right] \Psi_{\tilde{\mathbf{k}}}.\end{aligned}$$

We calculate the expectation value $\langle \overset{\leftrightarrow}{j} \rangle$ up to first order in \mathbf{A} (see details in appendix E), and find that the London kernel reads,

$$\begin{aligned}Q_{ij} &= \frac{e^2}{c} \sum_{\mathbf{k}} \sum_{\sigma=\pm 1} \\ &\quad \left\{ \frac{\beta}{2} [(\partial_i \epsilon_{\mathbf{k}})(\partial_j \epsilon_{\mathbf{k}}) + (\partial_i \Delta_{c\mathbf{k}})(\partial_j \Delta_{c\mathbf{k}})] \right. \\ &\quad \times \operatorname{sech}^2 \left(\frac{\beta E_{\mathbf{k},\sigma\mu}}{2} \right) \\ &\quad + \left(\frac{\epsilon_{\mathbf{k}}}{E_{\mathbf{k},\sigma\mu}} \partial_i \partial_j \epsilon_{\mathbf{k}} + \frac{\Delta_{c\mathbf{k}}}{E_{\mathbf{k},\sigma\mu}} \partial_i \partial_j \Delta_{c\mathbf{k}} \right) \frac{\sigma\mu + E_{\mathbf{k}}^*}{E_{\mathbf{k}}^*} \\ &\quad \left. \times \tanh \left(\frac{\beta E_{\mathbf{k},\sigma\mu}}{2} \right) \right\}, \quad (66)\end{aligned}$$

where $E_{\mathbf{k}}^* = \sqrt{\epsilon_{\mathbf{k}}^2 + \Delta_{c\mathbf{k}}^2}$ and

$$E_{\mathbf{k},\sigma\mu} = \left[\left(\sqrt{\epsilon_{\mathbf{k}}^2 + \Delta_{c\mathbf{k}}^2} + \sigma\mu \right)^2 + \Delta_s^2 \right]^{\frac{1}{2}}$$

is the generalized dispersion in the extended CDW band.

The non-local properties valid in the $q \rightarrow 0$ limit do not depend on the details of the cut-off Λ . For this reason, we are allowed to take Λ to infinity with no further consequences. However, the Green functions method leads to some spurious results in the ultraviolet if we do not take the full Brillouin zone into account. To see this, consider the illustrative case of the normal CDW band (65). After a suitable diagonalization into a particle-hole eigenstate basis with eigenvalues $\pm E_{\mathbf{k}}^* = \pm \sqrt{\epsilon_{\mathbf{k}}^2 + \Delta_{c\mathbf{k}}^2}$, we may write it into the form:

$$H_{CDW} = \sum_{\mathbf{k}} E_{\mathbf{k}}^* \bar{\Psi}^\dagger(\tilde{\mathbf{k}}) \eta_3 \bar{\Psi}(\tilde{\mathbf{k}}).$$

The London kernel of this problem can be derived directly from Eq. (66) by setting $\Delta_s = \mu = 0$, ignoring the $\Delta_{c\mathbf{k}}$ terms on it, and performing the substitution $\epsilon_{\mathbf{k}} \rightarrow E_{\mathbf{k}}$. It is immediate to see that in this case one has,

$$Q_{ij}^{CDW} = A_j \sum_{\mathbf{k}} \partial_i \left[(\partial_j E_{\mathbf{k}}) \tanh \left(\frac{\beta E_{\mathbf{k}}}{2} \right) \right],$$

resulting in a non-zero surface term for $i = j$, which diverges in the ultraviolet for any monotonically increasing $E_{\mathbf{k}}$. The integrability of the results derived by this method depends on the introduction of states in the entire Brillouin zone. In particular, we have that

$\langle j_i^{CDW} \rangle = 0$ (as expected) by assuming that the surface term cancels in the Brillouin zone because of its periodicity. In order to fix the spurious divergences, we follow an argument due to Lifshitz and Pitaevskii⁴⁴. Considering that the kernel for $\Delta_s = 0$ is zero, since no supercurrents are induced by the magnetic field, there is no physical result in subtracting from the SC kernel the normal phase kernel,

$$\langle j_i \rangle = [Q_{ij}(\Delta_s) - Q_{ij}(0)] A_j. \quad (67)$$

We may consider that the kernel above correctly incorporates the Brillouin zone effects, at least near the phase transition.

To analyze the spectral weight behavior due to the Meissner effect within the cone approximation $\epsilon_{\mathbf{k}} \sim v_F k_{\perp}$ and $\Delta_{c\mathbf{k}} \sim v_{\Delta} k_{\parallel}$, we calculate the London equation in two limits, near the normal-SC transition and at $T = 0$. Including the Brillouin zone $[-\frac{\pi}{d}, \frac{\pi}{d}]$ in the normal direction to the planes, with d the inter-plane distance, from Eq. (66) we have

$$Q_{\perp}(\Delta_s) = v_F^2 \frac{\beta}{2} \frac{e^2}{c} \sum_{\mathbf{k}, \sigma=\pm 1} \operatorname{sech}^2 \left(\frac{\beta E_{\mathbf{k},\sigma\mu}}{2} \right).$$

At $T = 0$, the kernel gives

$$Q_{\perp}(\Delta_s) - Q_{\perp}(0) \xrightarrow{T \rightarrow 0} -\frac{|\mu|}{d} \frac{e^2 v_F}{\pi v_{\Delta} c},$$

confirming the anomalous behavior detected by the f -sum rule (51) in the optical conductivity.

In the opposite limit, for $T \sim T_c$, the kernel in the strong coupling approximation ($\beta_c |\mu| \ll 1$) gives

$$Q_{\perp}(\Delta_s) - Q_{\perp}(0) \xrightarrow{T \rightarrow T_c} -\frac{\beta_c}{4d} \frac{v_F e^2}{\pi v_{\Delta} c} \left(1 + \mu^2 \frac{\beta_c^2}{4} \right) \Delta_s^2,$$

in agreement with the mean field result for the penetration depth $\lambda_{\perp} = \sqrt{c/[4\pi(Q_{\perp}(0) - Q_{\perp}(\Delta_s))]} \propto \Delta_s^{-1}$.

The dependence of the London kernel with μ and the temperature is shown in Fig 17. There is a clear suppression of the Meissner effect in the low temperature region, specially when the density of states in the Fermi surface nodes is close to zero. As we discussed previously in sec. VI, the opening of a SC gap in a nodal liquid possibly causes the spectral shift of high energy states beyond the cone cut-off α in the CDW band to the infrared. As we mentioned before, the spectral shift of the states below α (~ 60 meV) has actually been observed in the normal CDW phase of the TaSe₂²². More experimental studies are required to understand the SC phase properties in this crystal.

VIII. CONCLUSIONS

In this paper we have studied the thermodynamic and transport properties of a model proposed originally in

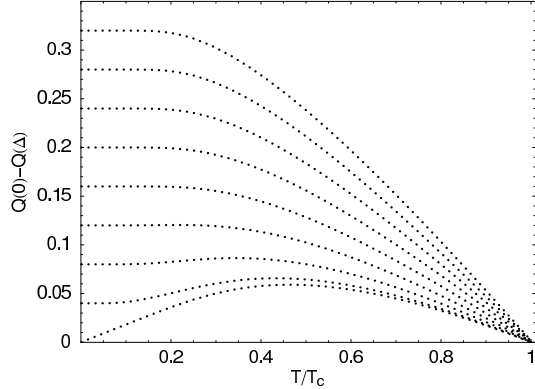


Figure 17: London kernel dependence with temperature in the cone approximation ($g/g_c = 1.1$). Plots for $0 \leq |\mu|/\alpha \leq 0.16$, from the bottom to the top, in fixed intervals of 0.02. $Q(0) - Q(\Delta_s)$ in units of $e^2 v_F \alpha / (2\pi d v \Delta c)$.

ref. [24] for the coexistence of a gapless CDW phase and a s -wave superconductor in TMD. While the lattice inversion symmetry is broken in the CDW distorted phase, as observed experimentally by neutron diffraction, we propose a pairing ansatz which also violates the time-reversal symmetry. According to the ansatz, the pairing of the electrons is mediated by virtual acoustic phonons *via* a piezoelectric coupling, and the center of mass momentum of the pairs equals the CDW wavevectors connecting different sheets of the TMD Fermi surface. This additional broken symmetry has dramatic consequences on the spin exchange interaction along the triple-CDW directions. The NMR pattern with respect to the directions of the Brillouin zone is expected to show a less intense nuclear spin attenuation rate along the CDW directions \mathbf{Q}_i and a more intense response in the normal directions to each of the three CDW vectors. In contrast to TaSe_2 , the quasiparticles of NbSe_2 are well defined in the Fermi-liquid regime. The SC phase of the NbSe_2 has been extensively studied and indicates that a conventional BCS description is warranted^{34,35,36}.

In contrast to the BCS theory, which is not critical, the gap equation (13) has a QCP in the critical coupling $g = g_c$ when the system exhibits particle-hole symmetry ($\mu = 0$). When this symmetry is broken, the SC gap Δ_s is strongly rescaled by μ as the coupling parameter is modified, and the QCP is suppressed. The scaling of the quantity Δ_s/μ follows two different coupling regimes: (i) “Fermi liquid” sector in weak coupling, for $g < g_c$, where Δ_s/μ flows to zero as $g \rightarrow 0$, and (ii) strong coupling marginal limit for $g > g_c$, where $\Delta_s/|\mu| \gg 1$. The specific heat jump is strongly attenuated in the particle-hole symmetric case (where $\Delta C_V/C_n = 0.35$), because of the low density of states at the Fermi energy. As expected, in the Fermi liquid regime we recover the jump of the BCS model $\Delta C_V/C_n = 1.43$.

We have observed several anomalous properties in the

transport. Unlike traditional one-band superconductors, the spectra for optical and thermal conductivities in the clean limit have an infrared peak due to the thermal channels of quasi-particle excitation. These channels involve thermal intraband excitations, promoting the electrons in the condensate to the empty states of the pocket, at the top of the lower band (see Fig. 12). The absorption window for this channel is limited to the pocket energy $2|\mu|$. A second kind of absorption channel is due to interband excitations, when a pair is broken as a result of the absorption of a photon. In this case, the electron is excited to the upper band, across the optical gap barrier $\omega_0 = 2\sqrt{\mu^2 + \Delta_s^2}$. The later type depends on the number of electrons in the condensate and is more effective at $T = 0$, except for a few channels at a given frequency ω_a which are abruptly suppressed by the temperature reduction (say, below T_a) because of the optical gap enlargement, that is, $\omega_a < \omega_0(T)$ for $T < T_a$. The thermal channels on the contrary vanish at $T = 0$ with no exception.

The optical conductivity has an absorption edge at ω_0 . The coherence factors are affected by the broken lattice inversion symmetry in the CDW phase. The f -sum rule reveals an anomalous suppression of the diamagnetic spectral weight, mainly for $\mu = 0$. This behavior is an evidence that there are missing high energy diamagnetic states in the SC phase, which would be attracted from the bottom to the top of the lower band by the opening of the SC gap. Close to the normal-SC phase transition, however, these states can be introduced by the same procedure that fixes the anomalous divergence of the London kernel in the ultraviolet, which is due to the absence of the Brillouin zone periodicity into the calculation. We have extended the calculation to a general CDW band where the loss of the crystal inversion symmetry is included by assumption.

In summary, we have presented a complete theory for s -wave superconductivity in nodal liquids. We have calculated the thermodynamics, the various response functions, and transport properties of this system and have shown that these quantities deviate strongly from the same properties in ordinary BCS superconductors when there is particle-hole symmetry. We believe our theory can be applied to some TMD, such as 2H-TaSe₂ or 2H-TaS₂, and our predictions can be checked experimentally.

Acknowledgments

B. U. and G. G. C. are indebted to E. Miranda for many helpful discussions. B. U. acknowledges FAPESP (Fundação de Amparo à Pesquisa do Estado de São Paulo), project number 00/06881-9, for the financial support. A.H.C.N. was partially supported through NSF grant DMR-0343790.

Appendix A: GAP EQUATION

In this appendix we derive Eq. (21)–(23). Applying the variable substitution $\nu = v_F \bar{k} + \sigma\mu$, the equation (13) can be written into the form

$$\begin{aligned} 1 &= \frac{gv_F}{4\pi v_\Delta} \sum_{\sigma=\pm 1} \int_0^{s_\sigma} d\bar{k} \frac{\bar{k}}{E_{\mathbf{k},\sigma\mu}} \tanh\left(\beta \frac{E_{\mathbf{k},\sigma\mu}}{2}\right) \\ &= \frac{g}{4\pi v_\Delta v_F} \left\{ \frac{4}{\beta} \ln \left[\cosh(\beta\alpha/2) \operatorname{sech} \left(\beta \sqrt{\Delta_s^2 + \mu^2}/2 \right) \right] \right. \\ &\quad \left. + \mu \int_{-\mu}^{\mu} d\nu \frac{1}{\sqrt{\nu^2 + \Delta_s^2}} \tanh\left(\beta \sqrt{\nu^2 + \Delta_s^2}\right) \right\}. \quad (\text{A1}) \end{aligned}$$

In the $|\mu|/\Delta_s \ll 1$ limit we find:

$$\begin{aligned} 1 &= \frac{g}{4\pi v_\Delta v_F} \left\{ \frac{4}{\beta} \ln \left[\frac{\cosh(\beta\alpha/2)}{\cosh(\beta\Delta_s/2)} \right] \right. \\ &\quad \left. + \frac{\mu^2}{\Delta_s} \tanh\left(\frac{\beta}{2}\Delta_s\right) \right\}, \end{aligned}$$

that is equivalent to Eq. (21). We notice, however, that the above expression remains valid at T_c (*i.e.* for finite μ and $\Delta_s \rightarrow 0$) if the strong coupling approximation $|\mu|/\Delta_{0\mu} \ll 1$ is satisfied.

We define $\alpha = 2\pi v_F v_\Delta / g_c$. Close to T_c , taking $\Delta_s \rightarrow 0$ we obtain,

$$\frac{2g_c}{g} = \frac{4}{\beta_c \alpha} \ln \left[\cosh\left(\frac{\beta_c \alpha}{2}\right) \right] + \frac{\mu^2 \beta_c}{2\alpha}.$$

The critical temperature for $g > g_c$ is,

$$T_c = \frac{1}{2k_B \ln 4} \left[\Delta_0 + \sqrt{\Delta_0^2 + \mu^2 \ln 4} \right], \quad (\text{A2})$$

where $\Delta_0 \equiv \Delta_s(T = 0, g, \mu = 0) = \alpha(1 - g_c/g)$. The expression that gives the critical dependence of the gap with temperature for $|\mu|/\Delta_{0\mu} \ll 1$ follows directly from the expansion of the gap equation (13) in terms of $\beta\Delta_s$.

To calculate the critical temperature in the weak coupling regime, we take $\Delta_s \rightarrow 0$ in Eq. (A1) leading to:

$$\begin{aligned} \frac{2g_c}{g} &= \frac{4}{\beta_c \alpha} \ln \left[\frac{\cosh(\beta_c \alpha/2)}{\cosh(\beta_c \mu/2)} \right] + \frac{2|\mu|}{\alpha} \left[\ln\left(\frac{\beta_c |\mu|}{2}\right) \right. \\ &\quad \left. \times \tanh\left(\frac{\beta_c \mu}{2}\right) - \int_0^{\beta_c |\mu|/2} d\zeta \frac{\ln \zeta}{\cosh^2 \zeta} \right] \end{aligned}$$

after integrating the second term of Eq. (A1) by parts. If $\beta_c |\mu| \gtrsim 4$, the integration above can be extended to the interval $[0, \infty]$,

$$\frac{2g_c}{g} = 2 + \frac{2|\mu|}{\alpha} \left[\ln\left(\frac{\beta_c |\mu| \gamma}{\pi}\right) - 1 \right].$$

In weak coupling ($|\mu|/\Delta_{0\mu} \gg 1$) the condition $\beta_c |\mu| \gg 1$ is easily satisfied. The equation above implies that

$$T_c = \frac{\mu \gamma}{k_B \pi} e^{\alpha(1-g_c/g)|\mu|^{-1}-1}, \quad (\text{A3})$$

where $\ln(\gamma) \approx 0.577$ is the Euler constant.

In the weak coupling regime, we can find the gap equation near the phase transition. For $\beta|\mu| \gg 1$, we use the power series expansion in $\beta\Delta_s \ll 1$ of the integral⁴⁵

$$\begin{aligned} \int_0^\mu d\nu \frac{\tanh\left(\frac{\beta}{2}\sqrt{\nu^2 + \Delta_s^2}\right)}{\sqrt{\nu^2 + \Delta_s^2}} &\sim \int_0^\mu d\nu \frac{1}{\nu} \tanh\left(\frac{\beta}{2}\nu\right) \\ &\quad - \frac{7\zeta(3)}{8} \frac{\beta^2 \Delta_s^2}{\pi^2} \end{aligned}$$

Expanding the gap equation (A1) in lowest order around β_c , we find

$$\Delta_s(T \rightarrow T_c, \mu) \xrightarrow{\beta_c \mu \gg 1} \frac{1}{\beta_c} \left[\frac{7\zeta(3)}{8\pi^2} + \frac{1}{2\beta_c^2 \mu^2} \right]^{-\frac{1}{2}} \sqrt{\frac{T_c - T}{T_c}}. \quad (\text{A4})$$

The weak coupling expansions given above are correct whenever $\tanh(\beta_c |\mu|/2) \sim 1$, or $\beta_c |\mu| \gtrsim 4$.

Appendix B: SPECIFIC HEAT

In this section we calculate explicitly the specific heat jump in the weak and strong coupling limits. The entropy of the problem is given by:

$$\begin{aligned} S &= -k_B \sum_{\mathbf{k}, \gamma, \sigma} \left[(1 - n_{\mathbf{k}, \sigma\mu}^\gamma) \ln(1 - n_{\mathbf{k}, \sigma\mu}^\gamma) \right. \\ &\quad \left. + n_{\mathbf{k}, \sigma\mu}^\gamma \ln n_{\mathbf{k}, \sigma\mu}^\gamma \right], \end{aligned}$$

where $n_{\mathbf{k}, \sigma\mu}^\gamma = (\mathrm{e}^{\gamma\beta E_{\mathbf{k}, \sigma\mu}} + 1)^{-1}$ is the Fermi-Dirac distribution, indexed by $\sigma = \pm 1$, and by the two branches of the cone. $\gamma = \pm 1$. The specific heat yields³³

$$\begin{aligned} C_V &= -\beta \frac{dS}{d\beta} \\ &= -k_B \beta \sum_{\mathbf{k}, \alpha, \sigma} \gamma \frac{\partial n_{\mathbf{k}, \sigma\mu}^\gamma}{\partial E_{\mathbf{k}, \sigma\mu}} \left(E_{\mathbf{k}, \sigma\mu}^2 + \frac{\beta}{2} \frac{d\Delta_s^2}{d\beta} \right) \quad (\text{B1}) \end{aligned}$$

At the phase transition, the specific heat jump reads:

$$\begin{aligned} \Delta C(\beta_c, \mu) &= \lim_{\beta \rightarrow \beta_c} \left[-k_B \frac{\beta_c^2}{2} \frac{d\Delta_s^2}{d\beta} \sum_{\mathbf{k}, \gamma, \sigma} \gamma \frac{\partial n_{\mathbf{k}, \sigma\mu}^\gamma}{\partial E_{\mathbf{k}, \sigma\mu}} \right] \\ &= \frac{k_B \beta_c^3}{8\pi v_\Delta v_F} \left. \frac{d\Delta_s^2}{d\beta} \right|_{\beta_c} \\ &\quad \times \sum_{\sigma=\pm 1} \int_0^\alpha d\epsilon \epsilon \operatorname{sech}^2 \left(\frac{\beta_c(\epsilon + \sigma\mu)}{2} \right). \end{aligned}$$

If $\beta_c \alpha \gtrsim 4$, we may extend the integration range to infinity. This integral can be evaluated in two limits, for

$\beta_c|\mu| \ll 1$ and $\beta_c|\mu| \gg 1$:

$$\Delta C(\beta, \mu) \longrightarrow \frac{k_B \beta_c}{2\pi v_\Delta v_F} \frac{d\Delta_s^2}{d\beta} \Big|_{\beta_c} \times \begin{cases} \ln 4 + \frac{\beta_c^2 \mu^2}{4} & , \text{ for } \beta_c|\mu| \ll 1 \\ \beta_c|\mu| & , \text{ for } \beta_c|\mu| \gg 1 \end{cases} \quad (\text{B2})$$

From Eq. (22) and (A2), we find:

$$\frac{d\Delta_s^2}{d\beta} \Big|_{\beta_c} = \begin{cases} \frac{4}{\beta_c^2} \left(\ln 4 + \frac{\beta_c^2 \mu^2}{4} \right) & , \text{ for } \beta_c|\mu| \ll 1 \\ \frac{1}{\beta_c^3} \left(\frac{7\zeta(3)}{8\pi^2} + \frac{1}{2\beta_c^2 \mu^2} \right)^{-1} & , \text{ for } \beta_c|\mu| \gg 1 \end{cases} \quad (\text{B3})$$

In the normal phase, the specific heat C_{Vn} is obtained from Eq. (B1),

$$C_{Vn}(\beta_c) = \frac{k_B \beta_c^2}{4\pi v_\Delta v_F} \sum_\sigma \int_0^\alpha d\epsilon \epsilon (\epsilon + \sigma\mu)^2 \times \operatorname{sech}^2 \left(\frac{\beta_c(\epsilon + \sigma\mu)}{2} \right).$$

Evaluating the integral gives:

$$C_{Vn}(\beta_c) \longrightarrow \frac{k_B}{2\pi v_F v_\Delta} \frac{1}{\beta_c^2} \times \begin{cases} 18\zeta(3) & , |\mu|\beta_c \ll 1 \\ \frac{2}{3}\pi^2 \beta_c |\mu| & , |\mu|\beta_c \gg 1. \end{cases} \quad (\text{B4})$$

Combining Eq. (B2), (B3) and (B4), we find

$$\frac{\Delta C_V}{C_{n,V}} \Big|_{T_c} = \begin{cases} \frac{2 \ln 4}{9\zeta(3)} \left(\ln 4 + \frac{\beta_c^2 \mu^2}{2} \right) & , |\mu|\beta_c \ll 1 \\ \frac{3}{2\pi^2} \frac{1}{\frac{7\zeta(3)}{8\pi^2} + \frac{1}{2\beta_c^2 \mu^2}} & , |\mu|\beta_c \gg 1. \end{cases} \quad (\text{B5})$$

Appendix C: SUSCEPTIBILITIES

We define the charge and spin susceptibilities from the imaginary time ordered correlation functions:

$$\chi^c(\mathbf{q}, i\omega) = - \int_0^\beta d\tau e^{i\omega\tau} \langle T_\tau [\rho(\mathbf{q}, \tau) \rho(-\mathbf{q}, 0)] \rangle \quad (\text{C1})$$

$$\chi_{ab}^s(\mathbf{q}, i\omega) = - \int_0^\beta d\tau e^{i\omega\tau} \langle T_\tau [S_a(\mathbf{q}, \tau) S_b(-\mathbf{q}, 0)] \rangle, \quad (\text{C2})$$

with ρ and S_a respectively as the charge and spin density operators defined by Eq. (29) and (34).

The optical, thermal and thermoelectric correlation functions are defined as,

$$\Pi_{ij}(\mathbf{q}, i\omega) = - \int_0^\beta d\tau e^{i\omega\tau} \langle j_i(\mathbf{q}, \tau) j_j(-\mathbf{q}, 0) \rangle \quad (\text{C3})$$

$$\Pi_{ij}^{EE}(\mathbf{q}, i\omega) = - \int_0^\beta d\tau e^{i\omega\tau} \langle j_i^E(\mathbf{q}, \tau) j_j^E(-\mathbf{q}, 0) \rangle \quad (\text{C4})$$

$$\Pi_{ij}^E(\mathbf{q}, i\omega) = - \int_0^\beta d\tau e^{i\omega\tau} \langle j_i^E(\mathbf{q}, \tau) j_j(-\mathbf{q}, 0) \rangle, \quad (\text{C5})$$

where \mathbf{j} is the electric current operator (44) and \mathbf{j}^E is the thermal current operator defined by Eq. (54).

Appendix D: HAMILTONIAN IN THE BALIAN-WERTHAMER SPACE

In this appendix we discuss Eq. (35). The BW space is introduced to extend the pairs space $(\mathbf{k} \uparrow, -\mathbf{k} \downarrow)$ to a larger one where the spin and momentum degrees of freedom are decoupled. The procedure rests on “duplicating” the Hamiltonian (keeping it invariant by summing in half Brillouin zone), interchange the order of the ψ fermionic operators in the duplicated term and explore the symmetry under the $\mathbf{k} \rightarrow -\mathbf{k}$ exchange in the k -sum. The CDW Hamiltonian in the BW space reads

$$\begin{aligned} H_{CDW} &= \sum_{\mathbf{k}, \sigma, a, b} v_F \psi_{a\sigma}^\dagger(\mathbf{k}) \bar{\mathbf{k}} \cdot \bar{\eta}^{ab} \psi_{b\sigma}(\mathbf{k}) \\ &= \frac{v_F}{2} \sum_{\mathbf{k}, a, b} \bar{\mathbf{k}} \cdot \left[\psi_{a\uparrow}^\dagger(\mathbf{k}) \bar{\eta}^{ab} \psi_{b\uparrow}(\mathbf{k}) \right. \\ &\quad + \psi_{a\downarrow}^\dagger(\mathbf{k}) \bar{\eta}^{ab} \psi_{b\downarrow}(\mathbf{k}) + \psi_{b\uparrow}(-\mathbf{k}) \bar{\eta}^{ba} \psi_{a\uparrow}^\dagger(-\mathbf{k}) \\ &\quad \left. + \psi_{b\downarrow}(-\mathbf{k}) \bar{\eta}^{ba} \psi_{a\downarrow}^\dagger(-\mathbf{k}) \right] \\ &= \sum_{\mathbf{k} \in \frac{1}{2}\text{B.Z.}} v_F \Psi^\dagger(\mathbf{k}) \sigma_0 \tau_0 \bar{\eta} \cdot \bar{\mathbf{k}} \Psi(\mathbf{k}), \end{aligned} \quad (\text{D1})$$

by the definition of the BW spinor (33).

The chemical potential term (6) can also be written as $-\mu \sum_{\mathbf{k} \in \frac{1}{2}\text{B.Z.}} \Psi^\dagger(\mathbf{k}) \sigma_0 \tau_3 \eta_0 \Psi(\mathbf{k})$. The pairing term can also be obtained with the use of the antisymmetric property of the Pauli matrix η_2 under the transposition $\eta_2^{ab} \rightarrow -\eta_2^{ba}$, namely,

$$\begin{aligned} H_P &= \sum_{\mathbf{k}, a, b} \Delta_s \psi_{a\uparrow}^\dagger(\mathbf{k}) \eta_2^{ab} \psi_{b\downarrow}^\dagger(-\mathbf{k}) + h.c. \\ &= \frac{1}{2} \sum_{\mathbf{k}, a, b} \Delta_s \left[\psi_{a\uparrow}^\dagger(\mathbf{k}) \eta_2^{ab} \psi_{b\downarrow}^\dagger(-\mathbf{k}) \right. \\ &\quad + \psi_{a\downarrow}(-\mathbf{k}) \eta_2^{ab} \psi_{b\uparrow}(\mathbf{k}) + \psi_{b\downarrow}^\dagger(\mathbf{k}) \eta_2^{ba} \psi_{a\uparrow}^\dagger(-\mathbf{k}) \\ &\quad \left. + \psi_{b\uparrow}(-\mathbf{k}) \eta_2^{ba} \psi_{a\downarrow}(\mathbf{k}) \right] \\ &= - \sum_{\mathbf{k} \in \frac{1}{2}\text{B.Z.}} \Delta_s \Psi^\dagger(\mathbf{k}) \sigma_3 \tau_1 \eta_2 \Psi(\mathbf{k}). \end{aligned} \quad (\text{D2})$$

Appendix E: LONDON KERNEL

In this appendix, we evaluate the London kernel (66). It can be derived from the calculation of the expectation

value of the current density operator,

$$\begin{aligned} \langle \overset{\leftrightarrow}{j}_i \rangle(\mathbf{k}) = \text{Tr} \sum_{\mathbf{k}} & \left[e \left(\partial_i \epsilon_{\mathbf{k}} - \frac{e}{c} A^j \partial_i \partial_j \epsilon_{\mathbf{k}} \right) \right. \\ & \times \langle \Psi^{\dagger}(\tilde{\mathbf{k}}) \tau_0 \eta_3 \Psi(\tilde{\mathbf{k}}) \rangle \\ & \left. + e \left(\partial_i \Delta_{c\mathbf{k}} - \frac{e}{c} A^j \partial_i \partial_j \Delta_{c\mathbf{k}} \right) \langle \Psi^{\dagger}(\tilde{\mathbf{k}}) \tau_0 \eta_1 \Psi(\tilde{\mathbf{k}}) \rangle \right] \end{aligned} \quad (\text{E1})$$

in first order in \mathbf{A} , where in our definition $\tilde{\mathbf{k}} = \mathbf{k} - \frac{e}{c} \tau_3 \mathbf{A}$. Expanding the Green function $\overset{\leftrightarrow}{G}(i\omega_n, \tilde{\mathbf{k}}) = (i\omega_n - \overset{\leftrightarrow}{\omega}_{\tilde{\mathbf{k}}})^{-1}$ up to leading order,

$$\begin{aligned} \text{Tr} \langle \Psi^{\dagger}(\tilde{\mathbf{k}}) \tau_{\mu} \eta_{\nu} \Psi(\tilde{\mathbf{k}}) \rangle = \frac{1}{\beta} \text{Tr} \sum_{\omega_n} & \tau_{\mu} \eta_{\nu} \overset{\leftrightarrow}{G}_0 \left[1 - \frac{e}{c} \overset{\leftrightarrow}{G}_0 \right. \\ & \times \left. (\partial_i \epsilon_{\mathbf{k}} \tau_0 \eta_3 + \partial_i \Delta_{c\mathbf{k}} \tau_0 \eta_1) A_i \right], \end{aligned}$$

where $\overset{\leftrightarrow}{G}_0$ is the Green function (12). The zeroth order terms are:

$$\begin{aligned} \text{Tr} \langle \Psi^{\dagger}(\tilde{\mathbf{k}}) \tau_0 \eta_3 \Psi(\tilde{\mathbf{k}}) \rangle_0 = \frac{1}{\beta} \text{Tr} \sum_{\omega_n} & \tau_0 \eta_3 \overset{\leftrightarrow}{G}_0 \\ = \epsilon_{\mathbf{k}} \sum_{\sigma=\pm 1} & \frac{\mu\sigma + E_{\mathbf{k}}^*}{E_{\mathbf{k}}^* E_{\mathbf{k},\sigma\mu}} \\ \times [n(E_{\mathbf{k},\sigma\mu}) - n(-E_{\mathbf{k},\sigma\mu})], \end{aligned} \quad (\text{E2})$$

and

$$\begin{aligned} \text{Tr} \langle \Psi^{\dagger}(\tilde{\mathbf{k}}) \tau_0 \eta_1 \Psi(\tilde{\mathbf{k}}) \rangle_0 = \Delta_{c\mathbf{k}} \sum_{\sigma=\pm 1} & \frac{\mu\sigma + E_{\mathbf{k}}^*}{E_{\mathbf{k}}^* E_{\mathbf{k},\sigma\mu}} \\ \times [n(E_{\mathbf{k},\sigma\mu}) - n(-E_{\mathbf{k},\sigma\mu})], \end{aligned} \quad (\text{E3})$$

where $E_{\mathbf{k}}^* \equiv \sqrt{\epsilon_{\mathbf{k}}^2 + \Delta_{c\mathbf{k}}^2}$ and

$$E_{\mathbf{k},\sigma\mu} = [(E_{\mathbf{k}}^* + \sigma\mu)^2 + \Delta_s^2]^{\frac{1}{2}}.$$

To first order we find, after a straightforward algebra:

$$\begin{aligned} \text{Tr} \langle \Psi^{\dagger}(\tilde{\mathbf{k}}) \tau_0 \eta_3 \Psi(\tilde{\mathbf{k}}) \rangle_1 = -\frac{e}{c} A_i \partial_i \epsilon_{\mathbf{k}} \frac{1}{\beta} \sum_{\omega_n} & \text{Tr} \left[(\overset{\leftrightarrow}{G}_0)^2 \right] \\ = -\frac{e}{c} \sum_{\sigma=\pm 1} & A^i (\partial_i \epsilon_{\mathbf{k}}) \\ \times \frac{\partial}{\partial E_{\sigma\mu}} & [n(E_{\mathbf{k},\sigma\mu}) - n(-E_{\mathbf{k},\sigma\mu})]. \end{aligned} \quad (\text{E4})$$

and

$$\begin{aligned} \text{Tr} \langle \Psi^{\dagger}(\tilde{\mathbf{k}}) \tau_0 \eta_1 \Psi(\tilde{\mathbf{k}}) \rangle_1 = -\frac{e}{c} \sum_{\sigma=\pm 1} & A^i (\partial_i \Delta_{c\mathbf{k}}) \\ \times \frac{\partial}{\partial E_{\sigma\mu}} & [n(E_{\mathbf{k},\sigma\mu}) - n(-E_{\mathbf{k},\sigma\mu})]. \end{aligned} \quad (\text{E5})$$

The London kernel (66) follows from the direct substitution of Eq. (E2), (E3), (E4) and (E5) into Eq. (E1), and by noting that the zero order current term,

$$\begin{aligned} \langle j \rangle_0 = \sum_{\sigma=\pm 1} \sum_{\mathbf{k}} & e (\epsilon_{\mathbf{k}} \partial_i \epsilon_{\mathbf{k}} + \Delta_{c\mathbf{k}} \partial_i \Delta_{c\mathbf{k}}) \frac{\mu\sigma + E_{\mathbf{k}}^*}{E_{\mathbf{k}}^* E_{\mathbf{k},\sigma\mu}} \\ \times [n(E_{\mathbf{k},\sigma\mu}) - n(-E_{\mathbf{k},\sigma\mu})] \end{aligned}$$

vanishes by symmetry when integrated over \mathbf{k} .

¹ R. L. Withers, and J. A. Wilson, J. Phys. C: Solid State Phys. **19**, 4809 (1986).
² J. A. Wilson, and A. D. Yoffe, Adv. Phys. **18**, 193 (1969); J. A. Wilson, F. J. DiSalvo e S. Mahajan, Adv. Phys. **24**, 117 (1975).
³ J. P. Tidman, O. Singh, and A. E. Curzon, Philos. Mag. **30**, 1191 (1974).
⁴ D. A. Whitney, R. M. Fleming, and R. V. Coleman, Phys. Rev. B **15**, 3405 (1977).
⁵ R. M. Fleming, D. E. Moncton, D. B. McWhan, and F. J. DiSalvo, Phys. Rev. Lett. **45**, 576 (1980).
⁶ D. B. McWhan, J. D. Axe, and R. Youngblood, Phys. Rev. B **24**, 5391 (1981).
⁷ T. Valla, A. V. Fedorov, P. D. Johnson, J. Xue, K. E. Smith, and F. J. DiSalvo, Phys. Rev. Lett. **85**, 4759 (2000).
⁸ R. A. Klemm, Physica C **341**, 839 (2000).
⁹ C. W. Chu, V. Diatschenko, C. Y. Huang, and F. J. DiSalvo, Phys. Rev. B **15**, 1340 (1977).
¹⁰ G. Wexler and A. M. Wooley, J. Phys. C **9**, 1185 (1976).
¹¹ J. A. Wilson, Phys. Rev. B **15**, 5748 (1977).
¹² D. E. Moncton, J. D. Axe, and F. J. DiSalvo, Phys. Rev. B **16**, 801 (1977).

¹³ W. Sacks, D. Roditchev, and J. Klein, Appl. Phys. A **66**, 925 (1998);
¹⁴ Th. Straub, Th. Finteis, R. Claessen, P. Steiner, S. Hufner, P. Blaha, C. S. Oglesby, and E. Bucher, Phys. Rev. Lett. **82**, 4504 (1999).
¹⁵ W. C. Tonjes, V. A. Greanya, Rong Liu, C. G. Olson, and P. Molinie, Phys. Rev. B **63**, 235101 (2001).
¹⁶ T. M. Rice, and G. M. Scott, Phys. Rev. Lett. **35**, 120 (1975); L. VanHove, Phys. Rev. **89**, 1189 (1953).
¹⁷ K. Rossnagel, O. Seifarth, L. Kipp, M. Skibowski, D. Voss, P. Kruger, A. Mazur, and J. Pollmann, Phys. Rev. B **64**, 235119 (2001).
¹⁸ O. Seifarth, S. Gliemann, M. Skibowski and L. Kipp, J. Electron Spectrosc. **137**, 675 (2004).
¹⁹ Rong Liu, C. G. Olson, W. C. Tonjes and R. F. Frindt, Phys. Rev. Lett. **80**, 5762 (1998).
²⁰ C. Wang, B. Giambattista, C. G. Slough, R. V. Coleman, and M. A. Subramanian, Phys. Rev. B **42**, 8890 (1990).
²¹ T. Valla, A. V. Fedorov, P. D. Johnson, P-A. Glans, C. McGuinness, K. E. Smith, E. Y. Andrei, and H. Berger, Phys. Rev. Lett. **92**, 86401 (2004).
²² V. Vescoli, L. Degiorgi, H. Berger, and L. Forro, Phys. Rev.

Lett. **81**, 453 (1998).

²³ P. B. Littlewood, and C. M. Varma, Phys. Rev B **46**, 405 (1992); C. M. Varma, P. B. Littlewood, S. Schmitt-Rink, E. Abrahams, and A. E. Ruckenstein, Phys. Rev Lett. **63**, 1996 (1989); **64**, 497(E) (1990).

²⁴ A. H. Castro Neto, Phys. Rev. Lett. **86**, 4382 (2001).

²⁵ M. Vojta, Y. Zhang, and S. Sachdev, Phys. Rev. B **62**, 6721 (2000).

²⁶ C. M. Varma, and W. Weber, Phys. Rev. Lett. **39**, 1094 (1977).

²⁷ D. P. DiVincenzo, and E. J. Mele, Phys. Rev. B **29**, 1685 (1984); J. Gonzalez, F. Guinea, and M. A. H. Vozmediano, Phys. Rev. Lett. **77**, 3589 (1996).

²⁸ D. Pines, and J. R. Schrieffer, Il Nuovo Cim. X, 3458 (1958).

²⁹ B. Uchoa, A. H. Castro Neto, and G. G. Cabrera, Phys. Rev. B **69**, 144512 (2004).

³⁰ P. W. Anderson, J. Phys. Chem. Solids **11**, 46 (1959).

³¹ P. W. Anderson, Phys. Rev. B **30**, 4000 (1984).

³² L. N. Cooper, Phys. Rev. **104**, 1189 (1956).

³³ M. Tinkham, *Introduction to Superconductivity* (McGraw-Hill, New York, 1996).

³⁴ R. A. Craven, and S. F. Meyer, Phys. Rev. B **16**, 4583 (1977).

³⁵ P. Garoche, J. J. Veyssié, P. Manuel, and P. Molinié, Solid State Comm. **19**, 455 (1976); R. E. Schwall, G. R. Stewart, and T. H. Geballe, J. Low Temp. Phys. **22**, 557 (1976).

³⁶ N. Kobayashi, K. Noto, and Y. Muto, J. Low Temp. Phys. **27**, 217 (1977); D. Sanchez, A. Junod, J. Muller, H. Berger, and F. Lütjény, Physica B **204**, 167 (1995).

³⁷ S. V. Dordevic, D. N. Basov, R. C. Dynes, B. Ruzicla, V. Vescoli, L. Degiorgi, H. Berger, R. Gaiò, L. Forrò, and E. Bucher, Eur. Phys. J. B **33**, 15 (2003).

³⁸ J. R. Schrieffer, *Theory of superconductivity* (Benjamin Inc., New York, 1964).

³⁹ G. D. Mahan, *Many-particle physics* (Plenum, New York, 1981).

⁴⁰ R. Balian, and N. R. Werthamer, Phys. Rev. **131**, 1553 (1963).

⁴¹ X. Yang, and C. Nayak, Phys. Rev. B **65**, 64523 (2002).

⁴² R. D. Parks, *Superconductivity* (Marcel Dekker Inc., New York, 1969) vol. 1, chap.2.

⁴³ M. E. Peskin, and D. V. Schroeder, *An introduction to quantum field theory* (Addison Wesley, Reading Mass., 1995), p.18.

⁴⁴ E. M. Lifshitz, and L. P. Pitaevskii, *Statistical physics* (Pergamon, Oxford, 1980) vol. 2, p. 213.

⁴⁵ A. A. Abrikosov, L. P. Gorkov, and I. E. Dzyaloshinskii, *Methods of quantum field theory in statistical physics* (Prentice Hall, New Jersey, 1964), p. 304.